Estimates of the density contrast at Earth's inner-core boundary beneath central Mexico

A Senior Project

presented to

the Faculty of the Physics Department

California Polytechnic State University, San Luis Obispo

In Partial Fulfillment

of the Requirements for the Degree

Bachelor of Science

by

Wade Kelley

June, 2012

Estimates of the density contrast at Earth's inner-core boundary beneath central Mexico

Abstract

Seismograms recorded in the western United States from a Guatemalan earthquake are examined for matching pairs of PKiKP and PcP waveforms for use in estimating the density contrast at earth's inner-core boundary via a PKiKP/PcP amplitude ratio analysis. Examination of waveforms from the SN, SC, TA, US and CI arrays finds 68 visually identifiable PKiKP and PcP pairs from which 17 were judged to be of sufficient quality (low signal-to-noise ratio) for use in the PKiKP/PcP amplitude ratio analysis. The epicentral distance range of the selected data spans epicentral distances from 22 – 37 degrees inside of which stations are generally in narrow epicentral range clusters. The observed amplitude ratios are generally higher than the AK135 Earth Model value of 0.6 g/cm^3, although the amplitude ratios do decrease with increasing epicentral distance. On average, the data suggests a density contrast at the inner-core boundary of 0.9 g/cm^3. However, substantial variation in the density contrast estimate occurs over narrow epicentral distance ranges. This observation is consistent with a recent model of the inner-core boundary surface as made up of a mosaic of patches where the liquid to solid phase transformation is solidified in some locations, and mushy mixed-phase layer in others.

Introduction

Earth's deepest phase transformation occurs at the inner-core boundary (ICB) at a depth of 5,150 km where the liquid outer-core becomes the solid inner-core. Earth's core is primarily made up of iron with several percent nickel and a few percent of "light elements." The light elements are thought to be silicon (Si) and oxygen (O) although potassium (K) is a candidate for a radioactive element in the core which may contribute to the core's energy budget [*Alfe et al.*, 1999]. Earth's inner-core grows as a result of freezing of the outer-core [*Bergman*, 2003]. During the freezing process light elements are preferentially partitioned into liquid outer-core, thereby releasing gravitational potential energy and is responsible for "compositional" in the outer. Convection of the liquid, electrically conducting, and rotating outer-core is responsible for the generation of earth's magnetic field. Thus earth's magnetic field in generated in a dynamo process, referred to as the geodynamo [*Braginsky and Roberts*, 1995; *Carrigan and Gubbins*, 1979; *Gubbins and Roberts*, 1987; *Merrill et al.*, 1998]. The power available via compositional convection for generation of the geodynamo is directly proportional to the density contrast at the inner-core boundary, $\Delta\rho_{ICB}$, and is given by $P_g = \Delta\rho_{ICB} \cdot (2 \times 10^{11})$ Watts [*Gubbins*, 1977]. Therefore estimates of $\Delta\rho_{ICB}$ are of primary importance in understanding the generation of earth's magnetic field. Standard one-dimensional earth models (e.g. AK135) report a value of $\Delta\rho_{ICB} = 0.6\ g/cm^3$. This value is derived from studies of normal modes sensitive to the ICB depth and represents a globally average value.

Local estimates of $\Delta\rho_{ICB}$ can be made with P-waves from earthquakes that reflect from both the core-mantle boundary (PcP) and the inner-core boundary (PKiKP) and are recorded on the same seismogram (Fig. 1) [*B.A. Bolt and Qamar*, 1970; *Cao and Romanowicz*, 2004; *Koper and Pyle*, 2004; *Shearer and Masters*, 1990; *Tkalcic et al.*, 2010; *Tkalčić et al.*, 2009]. Estimates of $\Delta\rho_{ICB}$ can be obtained by examining the PKiKP/PcP amplitude ratio against theoretical amplitude ratio predictions as a function of epicentral distance (Fig. 2) [*Bruce A. Bolt*, 1972]. Using the amplitude ratio method estimates of $\Delta\rho_{ICB}$ range from 0-1.8 g/cm^3. However values near 0.9 g/cm^3 are common in the amplitude ration literature, which is significantly higher than that obtained by the normal mode method [*B.A. Bolt and Qamar*, 1970; *Cao and Romanowicz*, 2004; *Koper and Pyle*, 2004; *Koper and Dombrovskaya*, 2005; *Krasnoshchekov et al.*, 2005; *Poupinet and Kennett*, 2004; *Shearer and Masters*, 1990; *Tkalcic et al.*, 2010; *Tkalčić et al.*, 2009].

In this study, the PKiKP/PcP amplitude ratios are obtained from seismograms in the western United States from several arrays recording a common earthquake with epicenter in Guatemala.

Data & Methods

The earthquake used in this study is a 2007 Guatemalan event (Fig. 1). After examining dozens of small seismic arrays in the United States and hundreds of individual seismograms, it was found that stations in the western US recorded contained higher quality and quantity of the necessary PKiKP and PcP waveform pairs on single seismograms (Fig. 1, 2). After applying a 0.5-2 Hz two-pole zero-phase Butterworth filter each seismogram was examined by eye for PKiKP and PcP arrivals near the theoretical arrival times of each waveform. In total, 35 seismograms were determined to have sufficiently clear PKiKP and PcP waveforms and low pre-arrival amplitude for computation of PKiKP/PcP amplitude rations (Fig. 3). From the set of 35, 25 seismograms generated amplitude ratios where the implied ICB density contrast was in the range of previously reported values of < 1.8 g/cm^3 (Fig. 2).

Amplitudes of PKiKP and PcP are measured from peak-to-trough and then used to compute the observed PKiKP/PcP ratio. Error bars for the observed ratio are estimated by computing the mean positive and negative amplitude of the seismograms in the 10 seconds prior to each waveform arrival. The PKiKP and PcP amplitudes are then perturbed by the corresponding mean positive of negative amplitude such that the ratio becomes maximally large or small (Fig. 2). Ratios and error estimates are then plotted against theoretical curves of PKiKP/PcP amplitude ratios as a function of distance (degrees) for a range of $\Delta\rho_{ICB}$ values. In this way it can be visually seen the range of ICB density contrasts implied by the data (Fig. 2). Amplitude ratios are also a function of epicentral distance. An amplitude ratio and corresponding epicentral distance which implies a value of $\Delta\rho_{ICB}$ > 1.8 g/cm^3 is here called anomalously large. The limit of 1.8 g/cm^3 is chosen because the previous literature in PKiKP/PcP amplitude ratios does not consider larger ICB density contrasts to be physically plausible.

Results

The plot of observed amplitude ratios and error bars as a function of epicentral distance for a range of $\Delta\rho_{ICB}$ values is seen in Figure 2. Although the data span a large epicentral range (17-37 degrees), most data appears in relatively narrow clusters of epicentral distance. All but three amplitude ratios plot above the $\Delta\rho_{ICB} = 0.6\ g/cm^3$ value from the AK135 earth model. It is noteworthy that in the epicentral distance range of approximately 32-33 degrees, amplitude ratios imply ICB density contrasts of $0.3 < \Delta\rho_{ICB} < 1.8$ g/cm^3 (Fig. 2). These results span stations in the CI, SN, and US arrays (Fig. 2).

With increasing epicentral distance, there is a weak trend of decreasing PKiKP/PcP amplitude ratio, however no particular theoretical curve of $\Delta\rho_{ICB}$ is strongly favored by the data (Fig. 2). Data within a particular array does not strongly follow a particular theoretical amplitude ratio curve (Fig. 2).

Figure 3 shows 3-D plots of the PKiKP, PcP amplitudes and corresponding amplitude ratio. These plots reveal that the PcP amplitude is the dominant modulator of the amplitude ratio. For example, it is the small PcP amplitude that generates anomalously large amplitude ratios of $\Delta\rho_{ICB} > 1.8\ g/cm^3$. Similarly, the cases of very large PcP amplitude are responsible for the smallest amplitude ratios. Conversely, larger values of PKiKP do not result in anomalously large values of $\Delta\rho_{ICB} > 1.8\ g/cm^3$.

In regions where several stations are geographically clustered and contained clear PKiKP observations, the seismograms were cross-correlated to optimally align the waveforms and produce a linear stack (Fig. 1, 4). A linear stack was computed at 8 stations of the CI array and 6 stations of SN array (Fig. 1,4). The result of linearly stacking the waveforms is an enhancement of the common signal (the PKiKP arrival) and a reduction of the supposedly uncorrelated signal in the seismograms prior to PKiKP. It is convenient that in the stations from the CI and SN arrays that the seismometers are of a common type and thus no correction for transfer function is needed. In both cases a very clear mean PKiKP waveform is obtained (Fig. 4). However even though the CI and SN stations are not too distant (Fig. 1), the mean PKiKP waveform is very distinct. In the case of the CI array the waveform has a prominent upward initial polarity while in the SN array stack the reverse is observed (Fig. 4). In addition the amplitude of the CI stack is only one-third the amplitude of the SN stack.

Discussion

The amplitude ratio observations in this study are typical of those observed in other amplitude ratio studies: (1) no single value of $\Delta\rho_{ICB}$ is preferred by the data, and (2) the data are somewhat clustered around a mean of $\Delta\rho_{ICB}$ = 0.9-1.2 g/cm^3 (Fig. 2) [*B.A. Bolt and Qamar*, 1970; *Cao and Romanowicz*, 2004; *Koper and Pyle*, 2004; *Koper and Dombrovskaya*, 2005; *Krasnoshchekov et al.*, 2005; *Poupinet and Kennett*, 2004; *Shearer and Masters*, 1990; *Tkalcic et al.*, 2010; *Tkalčić et al.*, 2009]. In addition, a wide range of implied values for $\Delta\rho_{ICB}$ are observed in narrow epicentral distance ranges, spanning more than one of the arrays (Fig. 2). Finally, the factor of three difference in the PKiKP linear stacks at two geographically close arrays (CI, SN) suggests that the P-wave reflectivity of the ICB can substantially vary over short distances on the ICB as seen by the closeness of the ICB sampling points of the two arrays (Fig. 1). However, PKiKP must travel twice through the complex core-mantle boundary region. This process must play a role in modulating its wave-shape

and amplitude. Indeed, the linear stack of the CI array data (Fig. 4) has lower frequency content. However, the extremely efficient reflection of PcP in this earthquake suggests that transmission of PKiKP at the core-mantle boundary is efficient as well suggesting that the ICB plays a significant role in modulating the amplitude and frequency content of PKiKP. Thus, the ICB must contain short wavelength variations in its reflectivity properties to account for these observations.

These observations support a previous model of the ICB which suggests that the ICB surface may be thought of as a "mosaic" [*Krasnoshchekov et al.*, 2005]. The mosaic model of the ICB surface hypothesizes that the ICB is made up of interspersed regions where the liquid-solid phase transformation is sharp (<10 km thick) and regions where the ICB is a mixed-phase layer with both solid and liquid components – a so-called mushy layer [*Bergman*, 2003; *Bergman and Fearn*, 1994; *Bergman et al.*, 2003; *Cormier*, 2007]. The wide range of values for $\Delta\rho_{ICB}$ over all epicentral distances as well as in narrow distance regions lends support to this model. In addition, the rapid change in frequency content of PKiKP over short distance scales (Fig. 4) supports a mosaic structural model at the ICB. Although complexity at the core-mantle boundary (CMB) may play a role in modulating the amplitude of PKiKP waves, this effect is likely small: one study of the core-mantle boundary region overlapping the present study area concluded that the velocity structure was adequately described by the IASP91 earth model [*Persh et al.*, 2001]. Because the upper-mantle raypaths beneath the CI and SN arrays is similar, it appears probable that the ICB surface is the primary cause of the observed amplitude variations.

Future work should focus on modeling the observed PKiKP stacks with synthetic seismograms over a large range of perturbations in $\Delta\rho_{ICB}$, $\Delta\rho_{CMB}$, and shear wave velocities at the ICB and CMB to determine probable values of these physical parameters and their contribution to reproducing the observed data.

Conclusions

This study has constrained the inner-core boundary density contrast beneath central Mexico to an average of 1.2 g/cm^3 with variation over short distance scales between 0.6 and 1.5 g/cm^3, in general agreement with previous amplitude ratio studies. The complexity in the observed PKiKP/PcP amplitude ratios as a function of both broad and narrow epicentral distances, as well as a factor of three variation in the PKiKP waveform stacks supports a mosaic model of the ICB where highly reflective patches are interspersed with a mixed-phase mushy layer.

References

Alfe, D., G. D. Price, and M. J. Gillan (1999), Oxygen in the Earth's Core: a first-principles study, *Physics of The Earth and Planetary Interiors*, *110*, 191-210.

Bergman, M. I. (2003), Solidification of the Earth's Core, *AGU Monographs, Geodynamics Series*, *31*.

Bergman, M. I., and D. R. Fearn (1994), Chimneys on the Earth's inner-outer core boundary?, *Geophysical Research Letters*, *21*, 477-480.

Bergman, M. I., S. Agrawal, M. Carter, and M. Macleod-Silbertstein (2003), Transverse solidification textures in hexagonal close-packed alloys, *Journal of Crystal Growth*, *255*, 204-211.

Bolt, B. A. (1972), The density distribution near the base of the mantle and near the earth's center, *Physics of The Earth and Planetary Interiors*, *5*, 301-311.

Bolt, B. A., and A. Qamar (1970), Upper bound to the density jump at the boundary of the Earth's core, *Nature*, *228*(5267), 148-150.

Braginsky, S. I., and P. H. Roberts (1995), Equations governing convection in earth's core and the geodynamo, *Geophysical & Astrophysical Fluid Dynamics*, *79*(1-4), 1-97.

Cao, A., and B. Romanowicz (2004), Constraints on density and shear velocity contrasts at the inner core boundary, *Geophysical Journal International*, *157*(3), 1146-1151.

Carrigan, C. R., and D. Gubbins (1979), The source of the Earth's magnetic field, edited, pp. 118-130, Scientific American, Inc., New York, NY.

Cormier, V. F. (2007), Texture of the uppermost inner core from forward- and back-scattered seismic waves, *Earth and Planetary Science Letters*, *258*(3-4), 442-453.

Gubbins, D. (1977), Energetics of the Earth's Core, *Journal of Geophysics*, *43*, 453-464.

Gubbins, D., and P. H. Roberts (1987), *Magnetohydrodynamics of the Earth's core*, 1-183 pp., Acad. Press, London.

Koper, K. D., and M. L. Pyle (2004), Observations of PKiKP/PcP amplitude ratios and implications for Earth structure at the boundaries of the liquid core, *Journal of Geophysical Research B: Solid Earth*, *109*(3), B03301 03301-03313.

Koper, K. D., and M. Dombrovskaya (2005), Seismic properties of the inner core boundary from PKiKP/P amplitude ratios, *Earth and Planetary Science Letters*, *237*(3-4), 680-694.

Krasnoshchekov, D. N., P. B. Kaazik, and V. M. Ovtchinnikov (2005), Seismological evidence for mosaic structure of the surface of the Earth's inner core, *Nature*, *435*(26), 483-487.

Merrill, R. T., M. W. McElhinney, and P. L. McFadden (1998), The Magnetic Field of the Earth, *Academic Press*.

Persh, S. E., J. E. Vidale, and P. S. Earle (2001), Absence of short-period ULVZ precursors to PcP and ScP from two regions of the CMB, *Geophysical Research Letters*, *28*(2), 387-390.

Poupinet, G., and B. L. N. Kennett (2004), On the observation of high frequency PKiKP and its coda in Australia, *Physics of the Earth and Planetary Interiors*, *146*(3-4), 497-511.

Shearer, P., and G. Masters (1990), The density and shear velocity contrast at the inner core boundary, *Geophysical Journal International*, *102*(2), 491-498.

Tkalcic, H., V. F. Cormier, B. L. N. Kennett, and K. He (2010), Steep reflections from the earth's core reveal small-scale heterogeneity in the upper mantle, *Physics of The Earth and Planetary Interiors*, *178*(1-2), 80-91.

Tkalčić, H., B. L. N. Kennett, and V. F. Cormier (2009), On the inner–outer core density contrast from PKiKP/PcP amplitude ratios and uncertainties caused by seismic noise, *Geophysical Journal International*, *179*(1), 425-443.

Figures

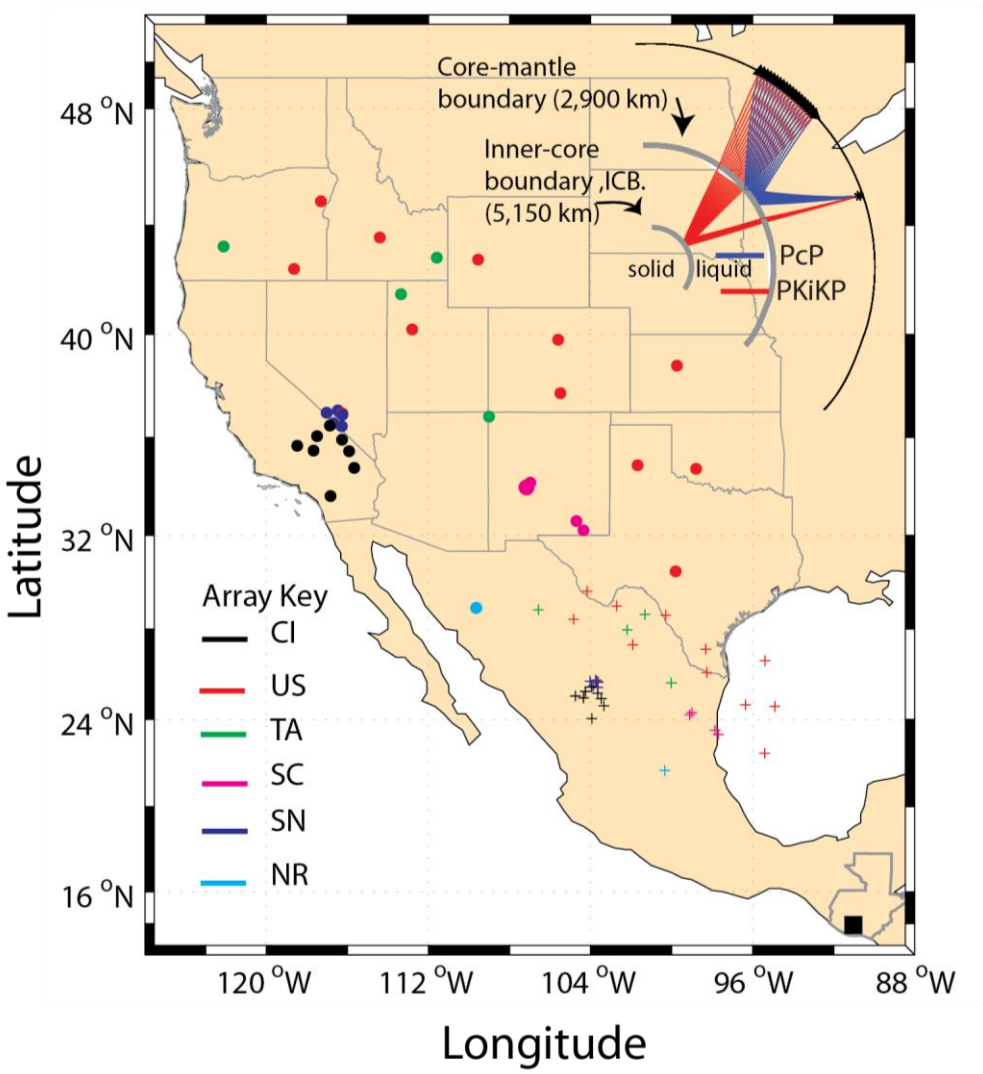

Figure 1. Locations of seismic arrays, ICB reflection points and earthquake epicenter. The color-coded circles are the seismic stations at various arrays, "+" signs are the P-wave reflection points on the inner-core boundary (ICB), and the black square is the epicenter (14.4°, -91.03°) of the July 23, 2007 (origin time 22:30:09), 113-km deep Guatemalan earthquake used in this study. Inset (top right): raypaths of PKiKP waves (red) and PcP waves (blue) from source to an array of receivers. Also noted is the liquid-solid interface at the ICB.

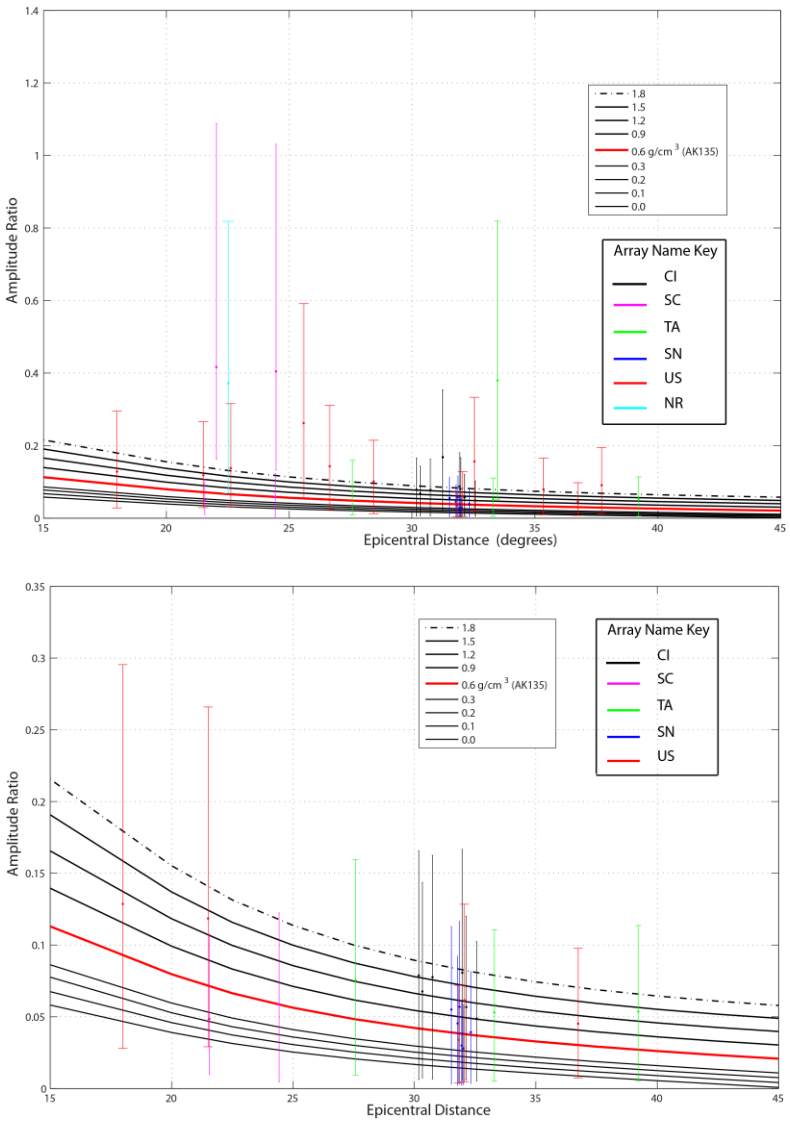

Figure 2. Observed PKiKP/PcP amplitude ratios vs. $\Delta\rho_{ICB}$ and epicentral distance. Top: Full dataset from Figure 1 and Appendix 1. Bottom: Subset of data with amplitude ratios implying $\Delta\rho_{ICB} < 1.8$ g/cm^3. Observed PKiKP/PcP amplitude ratios and error bars are plotted against epicentral distance for a range of $\Delta\rho_{ICB}$ values. The solid red line is the reference AK135 value of $\Delta\rho_{ICB}$. Black lines are theoretical amplitude ratios for other values of $\Delta\rho_{ICB}$. Top dashed line corresponds to $\Delta\rho_{ICB}$=1.8 g/cm^3, the largest accepted value from the totality of previous studies.

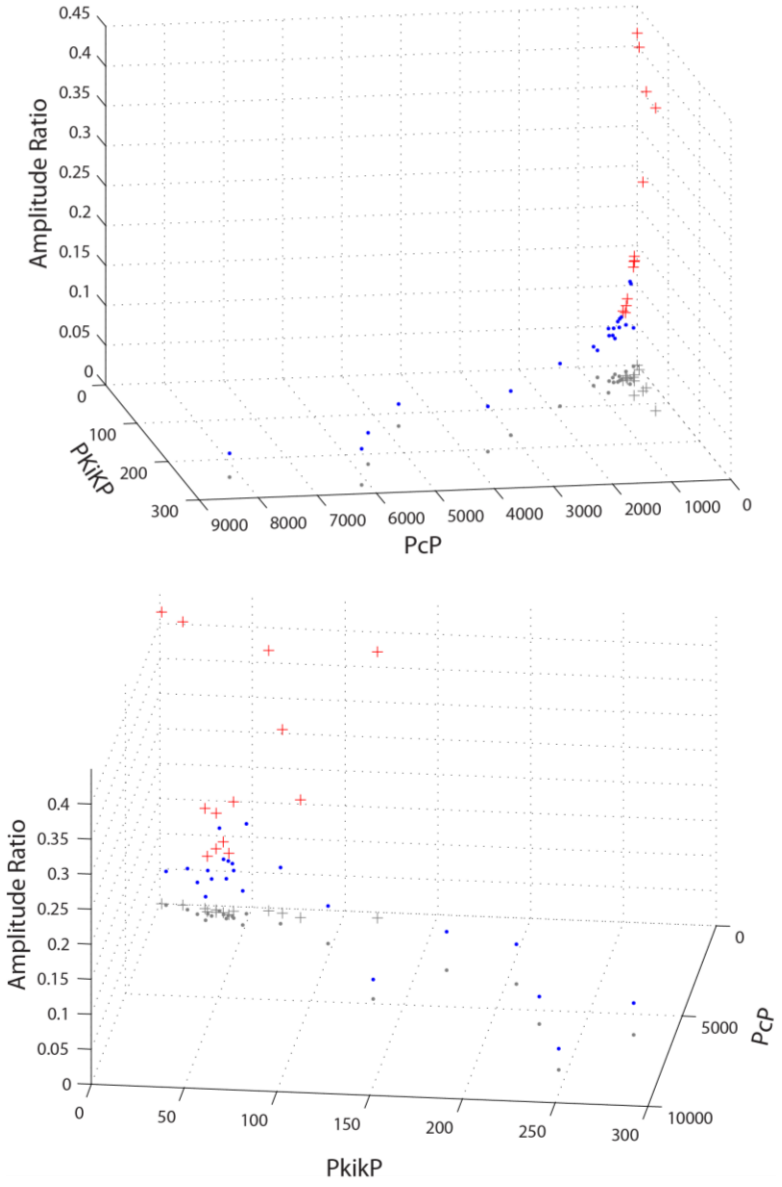

Figure 3. PKiKP/PcP amplitude ratio as a function of PKiKP and PcP amplitudes. Top: view from PcP axis. Bottom: view from PKiKP axis. Gray symbols are (PKiKP,PcP) coordinate pairs (in units of *counts*). Gray circles are amplitude ratios which plot below $\Delta\rho_{ICB} = 1.8\ g/cm^3$ and gray plus signs are amplitude ratios plotting above $\Delta\rho_{ICB} = 1.8\ g/cm^3$. Red and blue circles are those ratios which plot above and below, respectively, $\Delta\rho_{ICB} = 1.8\ g/cm^3$.

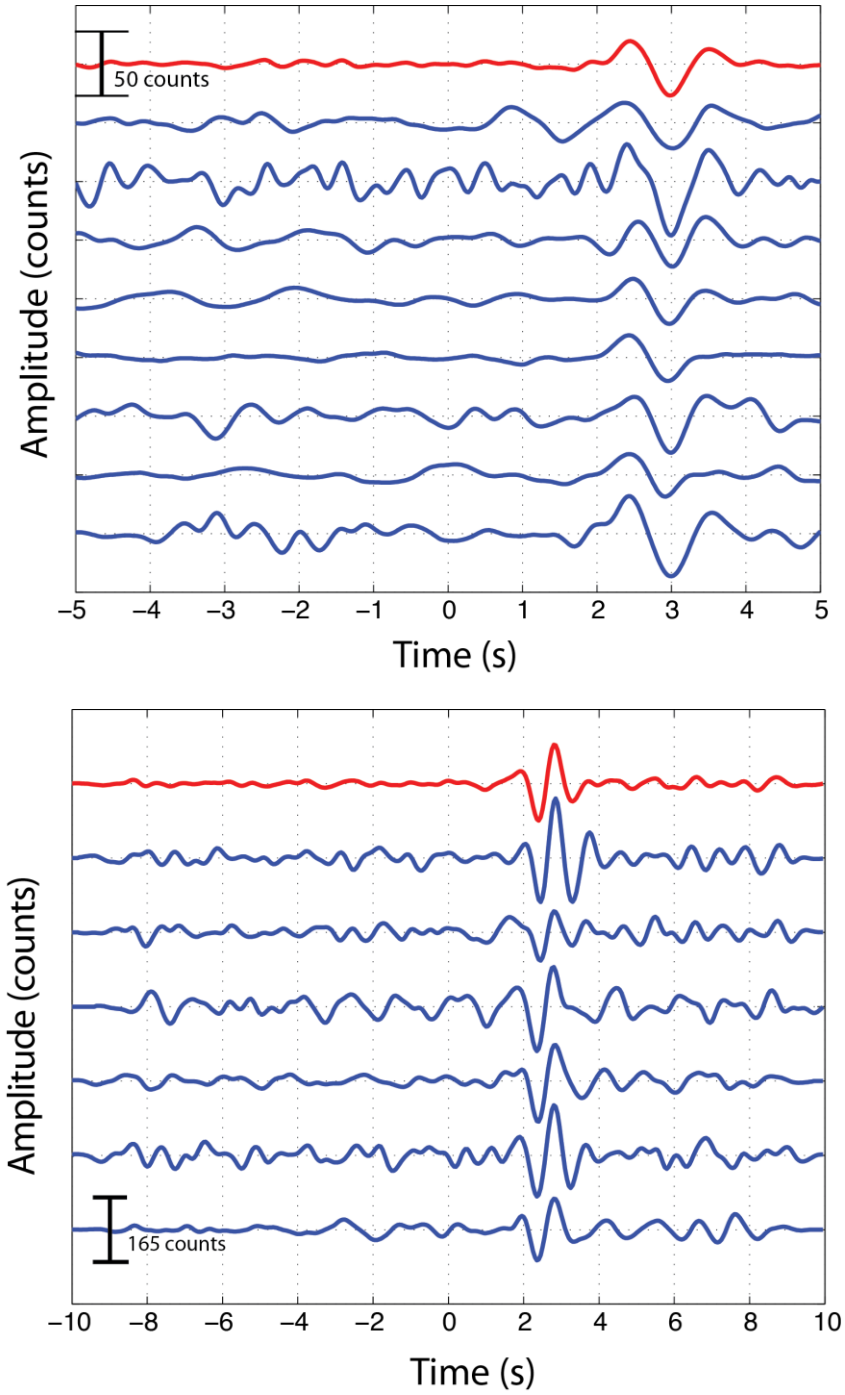

Figure 4. Linear stacks of PKiKP waveforms at CI and SN. Linear stack of cross-correlated PKiKP seismograms at the CI array (top) and SN array (bottom). Individual seismograms are in blue and the linear stack is in red. In each plot the bottom trace was used as the reference trace for cross-correlation, thus the time axis is only accurate for the bottom trace, which shows the arrival time residual of the PKiKP phase relative to the AK135 earth model theoretically predicted arrival time.

Appendices

Appendix 1: Seismograms from stations shown in Figure 1.

Appendix 2: Array and station location data.

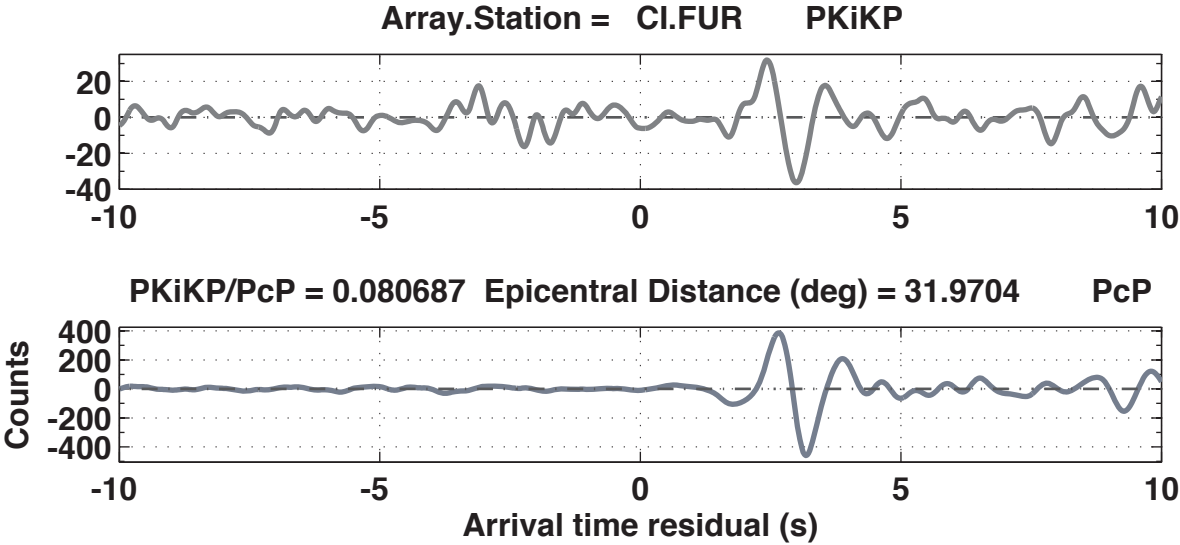
Array.Station = CI.FUR PKiKP
20
0
-20
-40
-10
-5
0
5
10
PKiKP/PcP = 0.080687 Epicentral Distance (deg) = 31.9704 PcP
400
200
0
-200
-400
Counts
-10
-5
0
5
10
Arrival time residual (s)

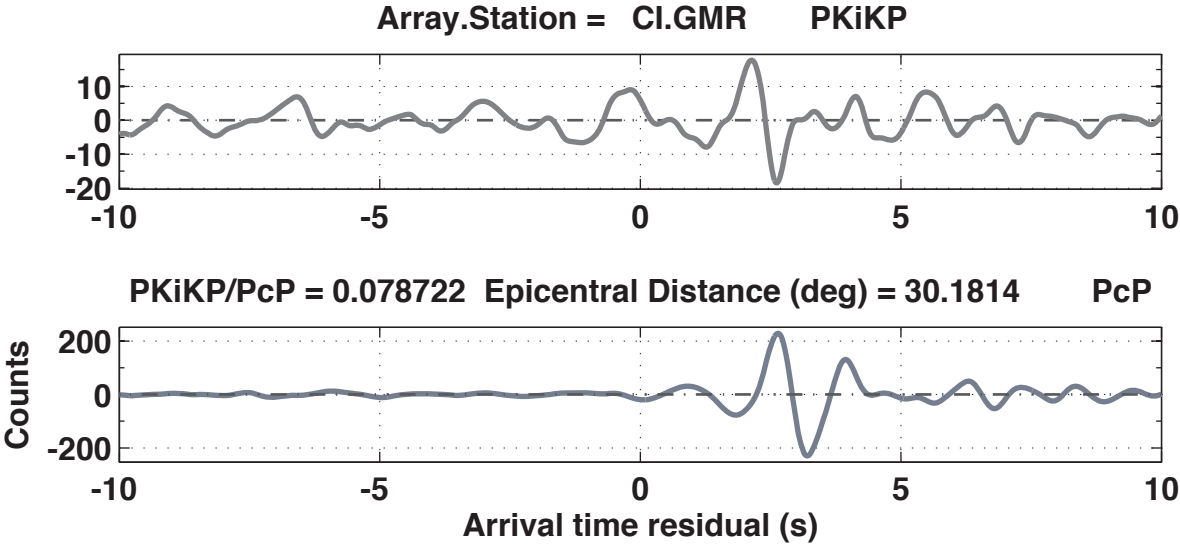
Array.Station = CI.GMR PKiKP
10
0
-10
-20
-10
-5
0
5
10
PKiKP/PcP = 0.078722 Epicentral Distance (deg) = 30.1814 PcP
Counts
200
0
-200
-10
-5
0
5
10
Arrival time residual (s)

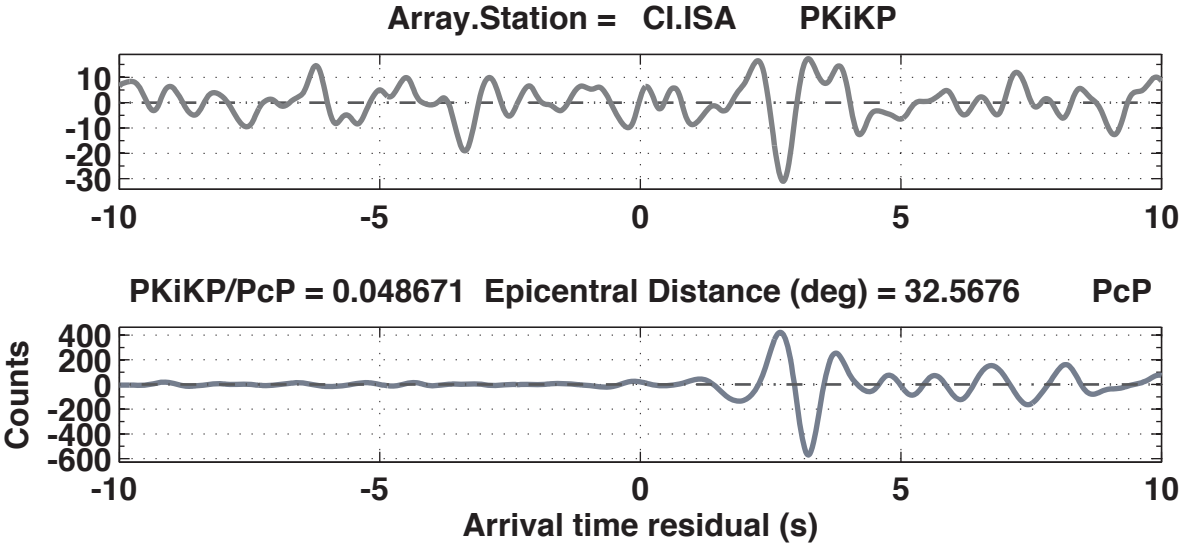
Array.Station = CI.ISA PKiKP
10
0
-10
-20
-30
-10
-5
0
5
10
PKiKP/PcP = 0.048671 Epicentral Distance (deg) = 32.5676 PcP
400
200
0
-200
-400
-600
Counts
-10
-5
0
5
10
Arrival time residual (s)

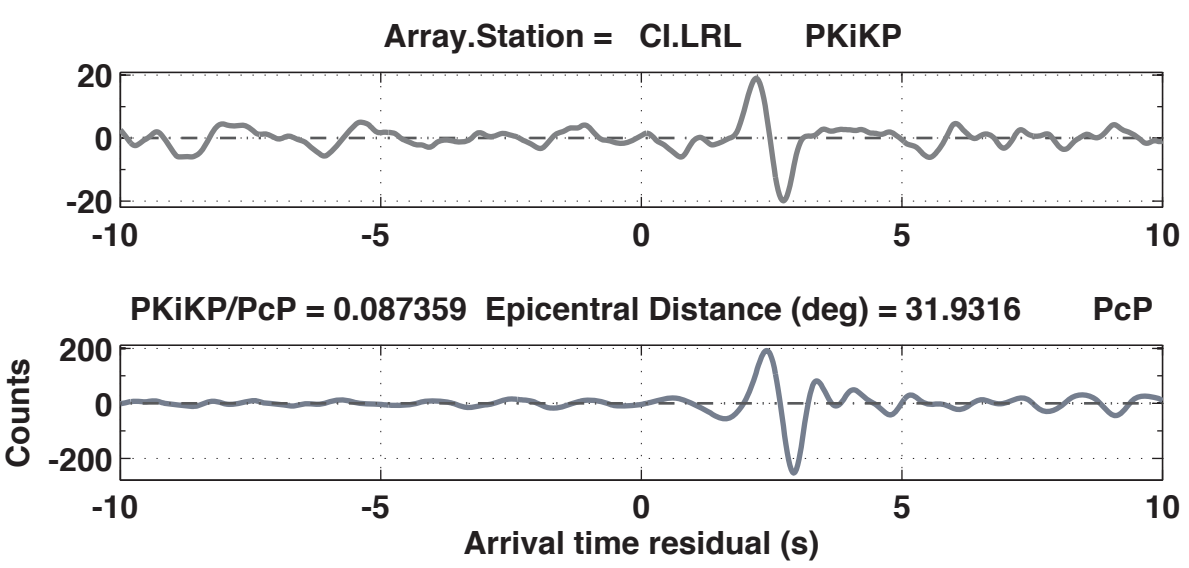
Array.Station = CI.LRL PKiKP
20
0
-20
-10
-5
0
5
10
PKiKP/PcP = 0.087359 Epicentral Distance (deg) = 31.9316 PcP
200
0
-200
Counts
-10
-5
0
5
10
Arrival time residual (s)

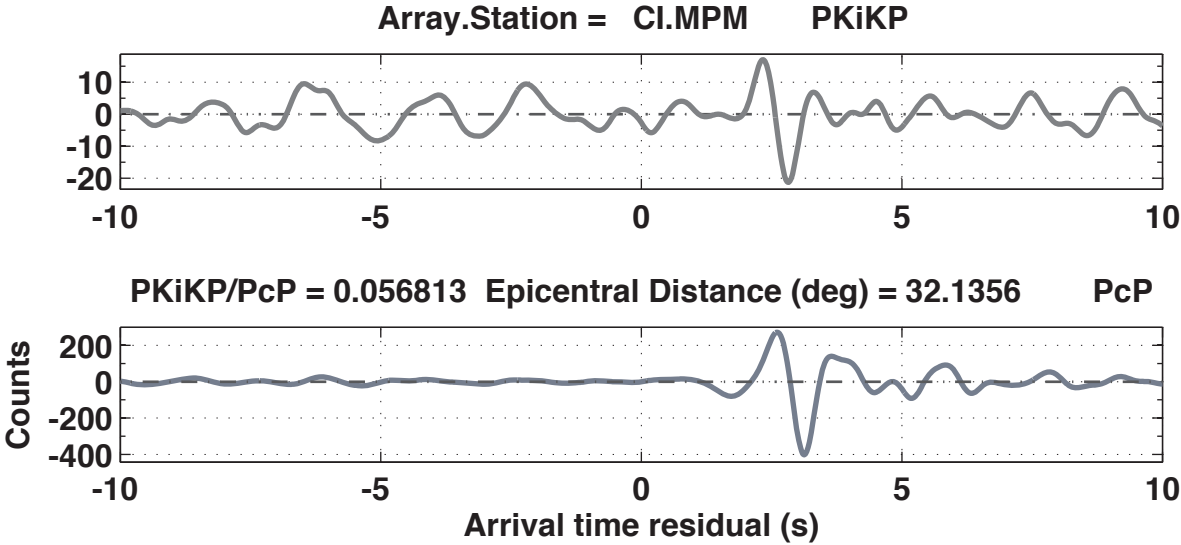
Array.Station = CI.MPM PKiKP
10
0
-10
-20
-10
-5
0
5
10
PKiKP/PcP = 0.056813 Epicentral Distance (deg) = 32.1356 PcP
Counts
200
0
-200
-400
-10
-5
0
5
10
Arrival time residual (s)

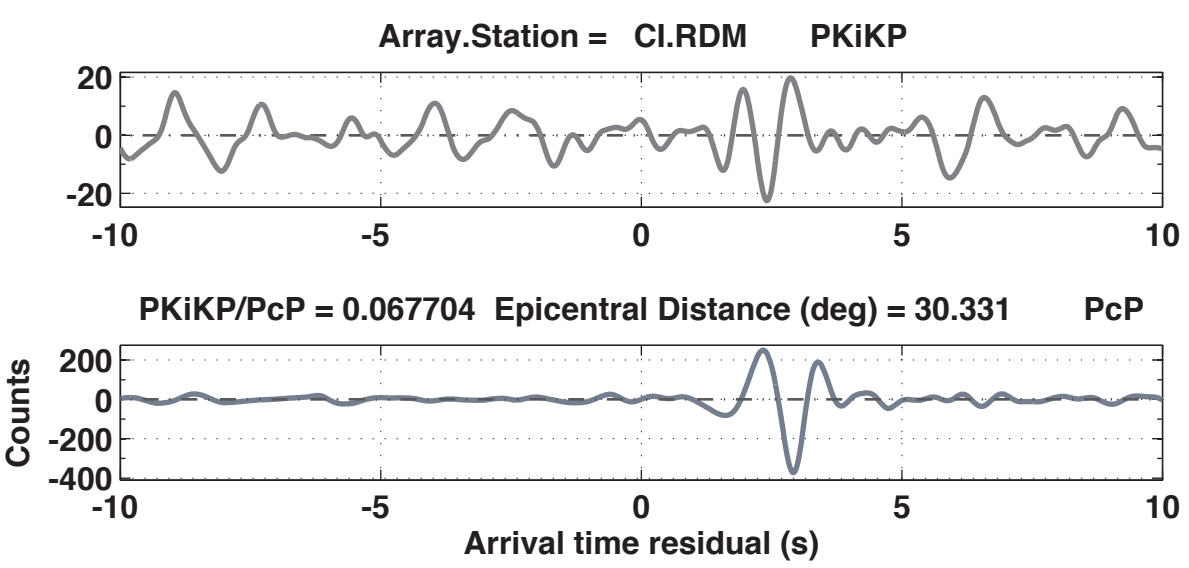
Array.Station = CI.RDM PKiKP
20
0
-20
-10
-5
0
5
10
PKiKP/PcP = 0.067704 Epicentral Distance (deg) = 30.331 PcP
Counts
200
0
-200
-400
-10
-5
0
5
10
Arrival time residual (s)

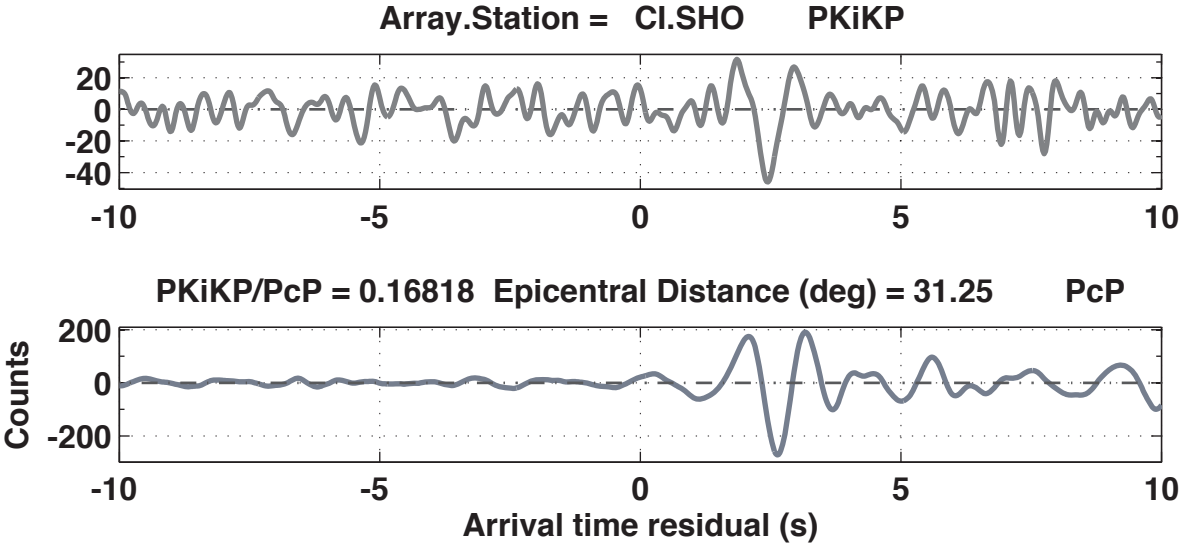
Array.Station = CI.SHO PKiKP
20
0
-20
-40
-10
-5
0
5
10
PKiKP/PcP = 0.16818 Epicentral Distance (deg) = 31.25 PcP
Counts
200
0
-200
-10
-5
0
5
10
Arrival time residual (s)

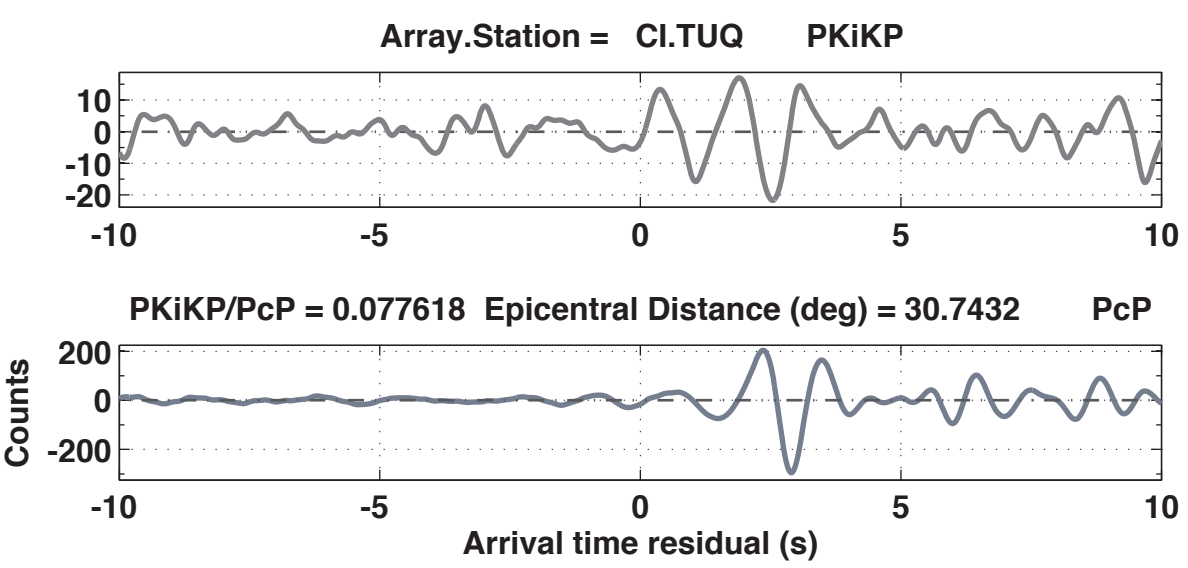
Array.Station = CI.TUQ PKiKP
10
0
-10
-20
-10
-5
0
5
10
PKiKP/PcP = 0.077618 Epicentral Distance (deg) = 30.7432 PcP
200
0
-200
Counts
-10
-5
0
5
10
Arrival time residual (s)

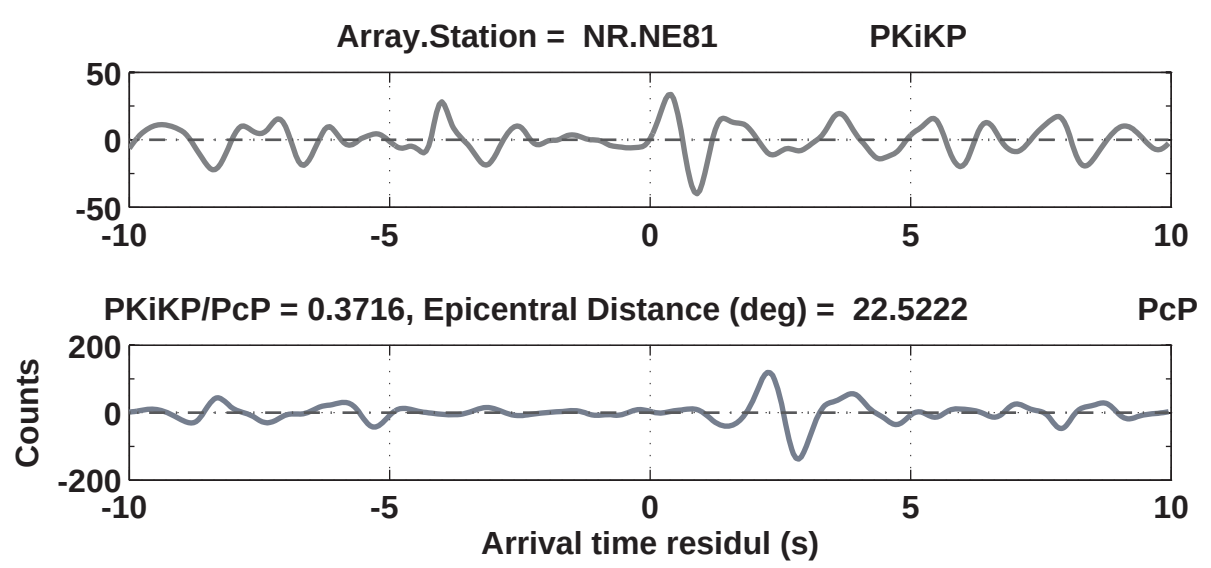
Array.Station = NR.NE81
PKiKP
50
0
-50
-10
-5
0
5
10
PKiKP/PcP = 0.3716, Epicentral Distance (deg) = 22.5222
PcP
200
0
-200
Counts
-10
-5
0
5
10
Arrival time residul (s)

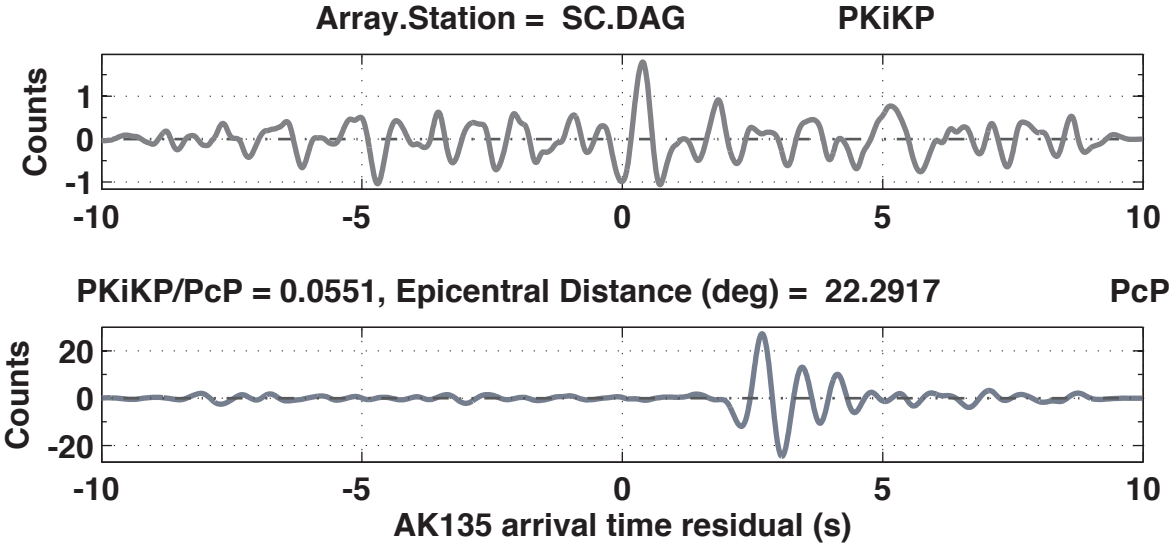
Array.Station = SC.DAG
PKiKP
Counts
1
0
-1
-10
-5
0
5
10
PKiKP/PcP = 0.0551, Epicentral Distance (deg) = 22.2917
PcP
Counts
20
0
-20
-10
-5
0
5
10
AK135 arrival time residual (s)

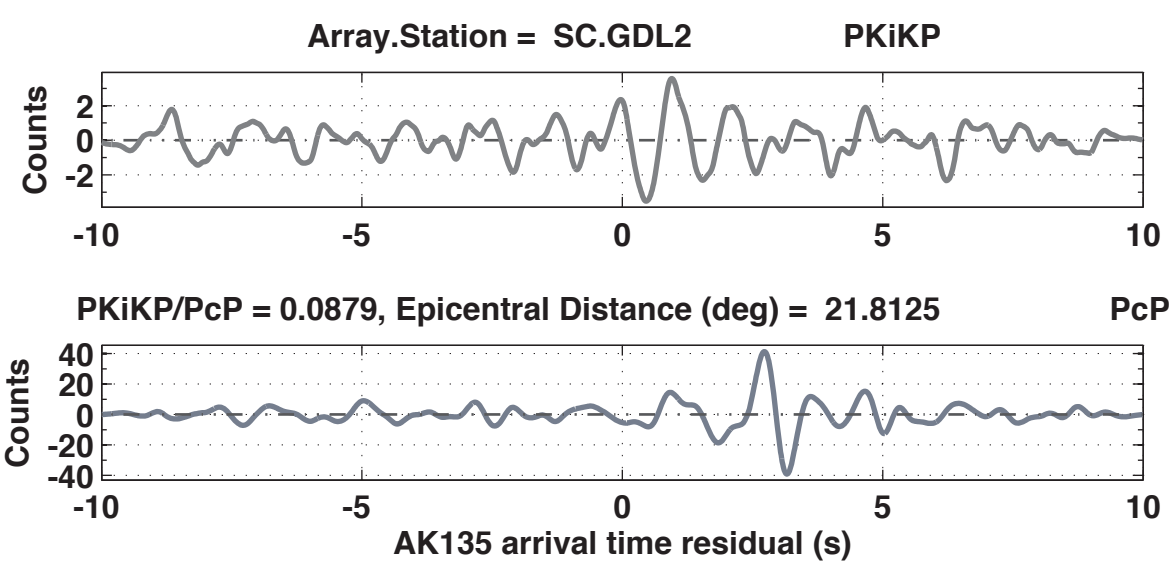
Array.Station = SC.GDL2
PKiKP
Counts
2
0
-2
-10
-5
0
5
10
PKiKP/PcP = 0.0879, Epicentral Distance (deg) = 21.8125
PcP
Counts
40
20
0
-20
-40
-10
-5
0
5
10
AK135 arrival time residual (s)

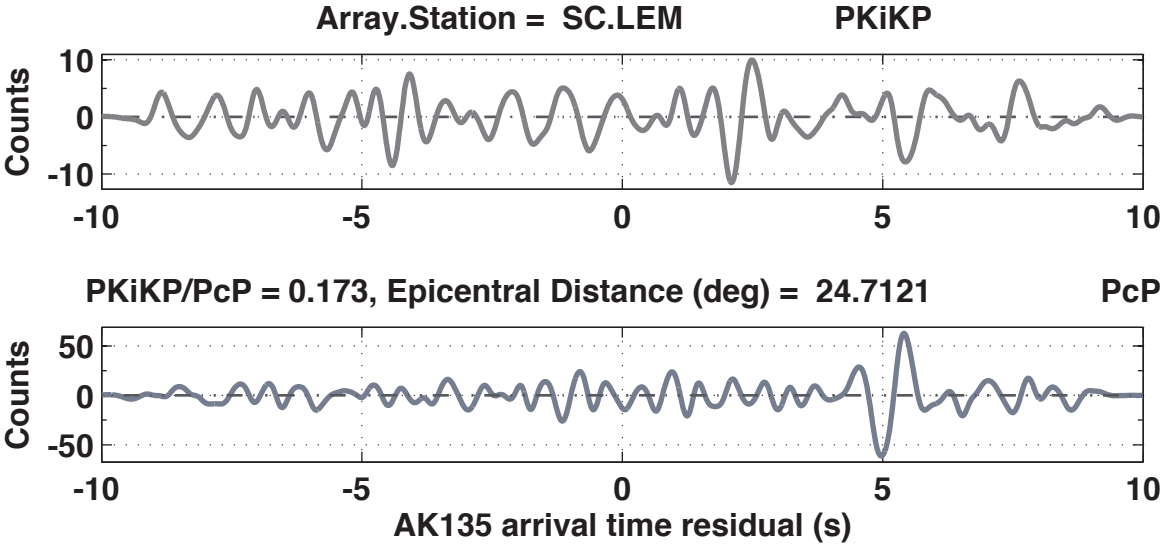
Array.Station = SC.LEM
PKiKP
Counts
10
0
-10
-10
-5
0
5
10
PKiKP/PcP = 0.173, Epicentral Distance (deg) = 24.7121
PcP
Counts
50
0
-50
-10
-5
0
5
10
AK135 arrival time residual (s)

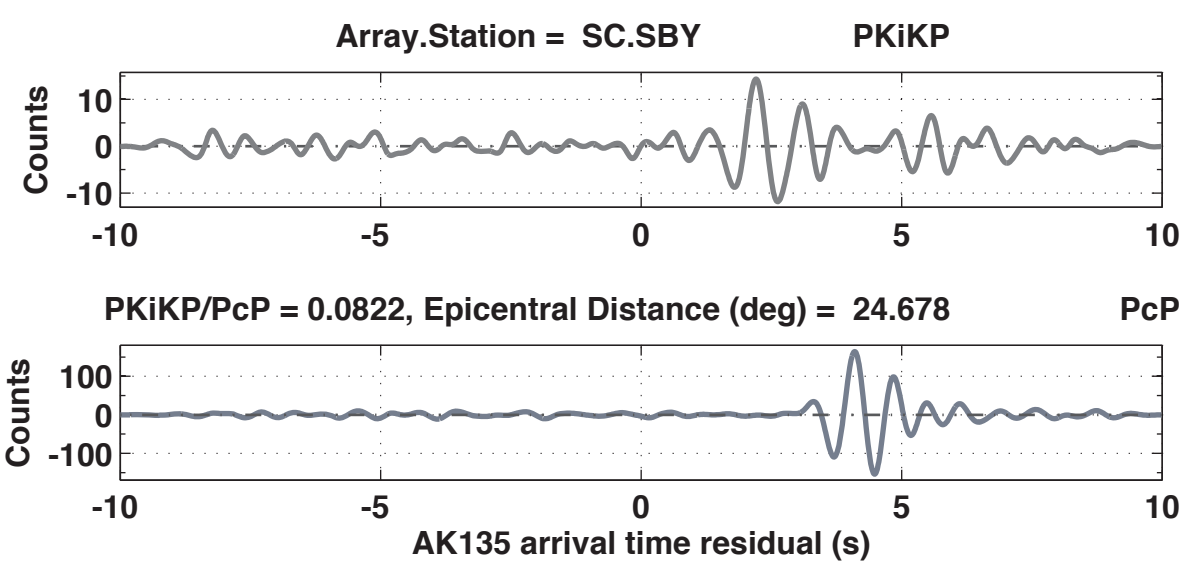
Array.Station = SC.SBY
PKiKP
Counts
10
0
-10
-10
-5
0
5
10
PKiKP/PcP = 0.0822, Epicentral Distance (deg) = 24.678
PcP
Counts
100
0
-100
-10
-5
0
5
10
AK135 arrival time residual (s)

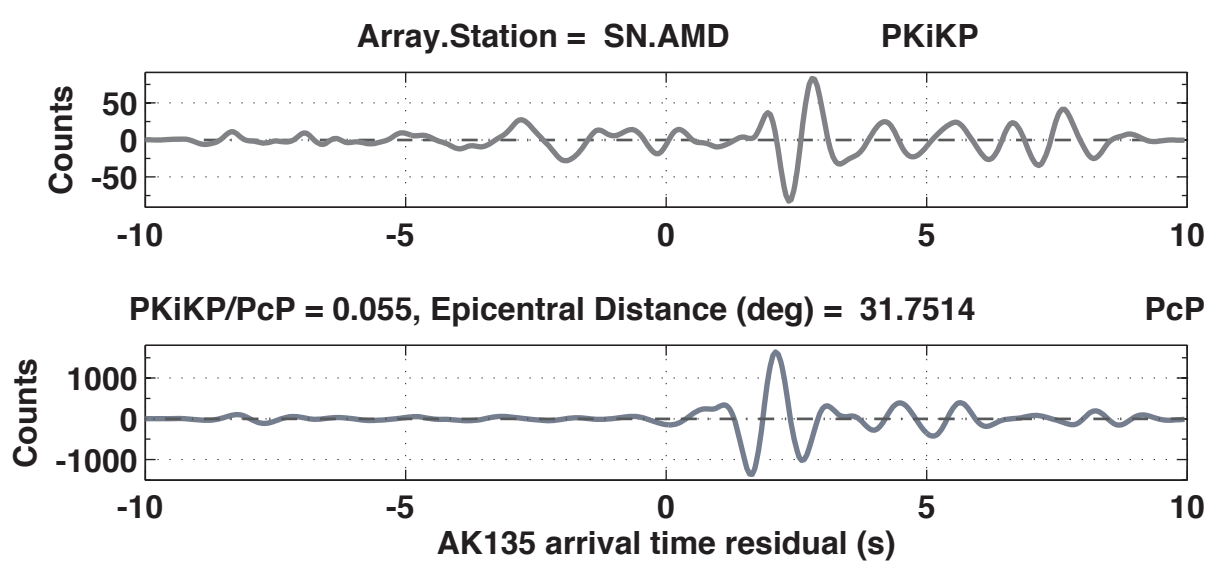
Array.Station = SN.AMD
PKiKP
Counts
50
0
-50
-10
-5
0
5
10
PKiKP/PcP = 0.055, Epicentral Distance (deg) = 31.7514
PcP
Counts
1000
0
-1000
-10
-5
0
5
10
AK135 arrival time residual (s)

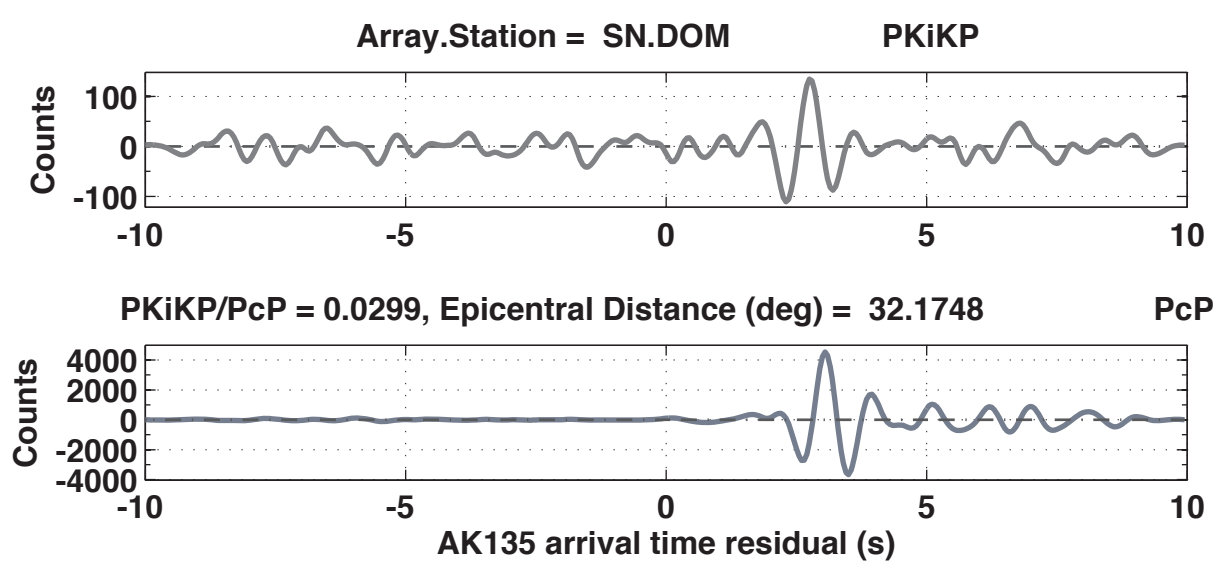
Array.Station = SN.DOM
PKiKP
Counts
100
0
-100
-10
-5
0
5
10
PKiKP/PcP = 0.0299, Epicentral Distance (deg) = 32.1748
PcP
Counts
4000
2000
0
-2000
-4000
-10
-5
0
5
10
AK135 arrival time residual (s)

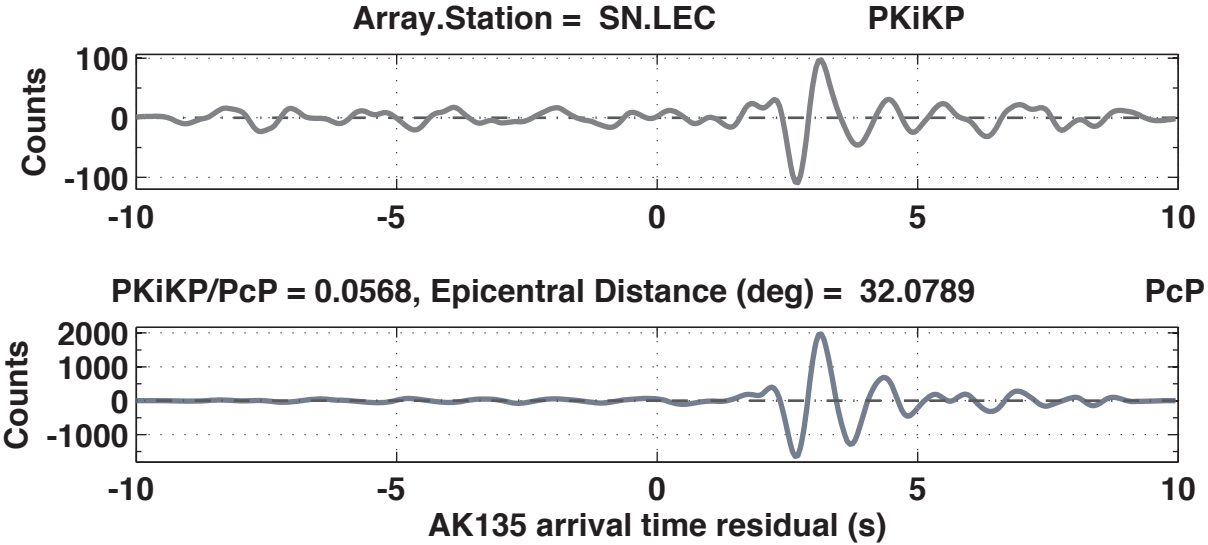
Array.Station = SN.LEC
PKiKP
Counts
100
0
-100
-10
-5
0
5
10
PKiKP/PcP = 0.0568, Epicentral Distance (deg) = 32.0789
PcP
Counts
2000
1000
0
-1000
-10
-5
0
5
10
AK135 arrival time residual (s)

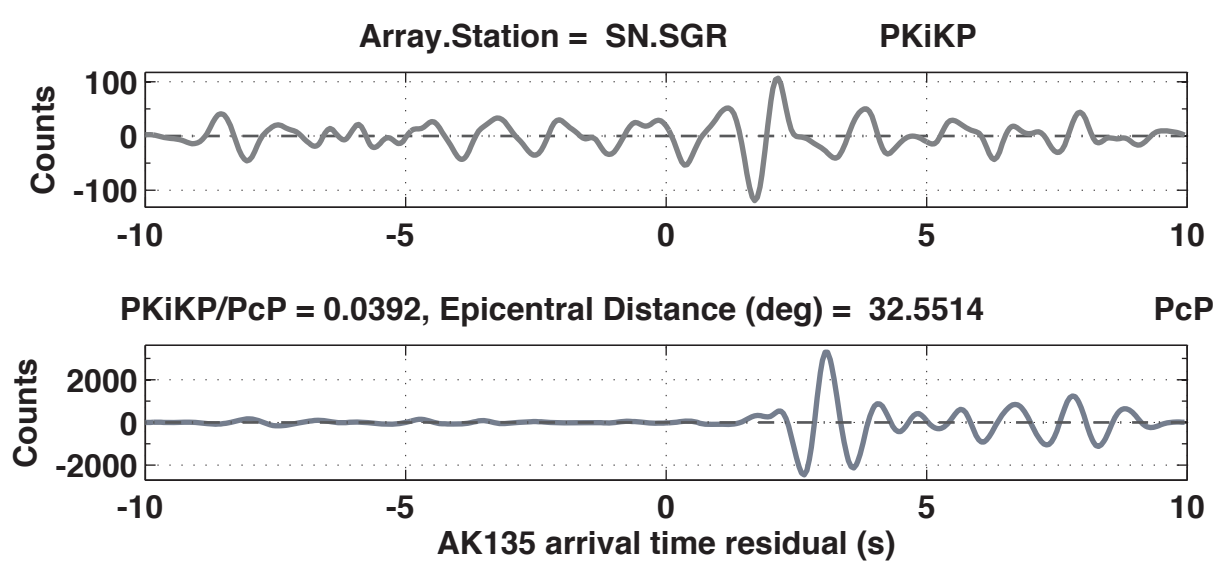
Array.Station = SN.SGR
PKiKP
Counts
100
0
-100
-10
-5
0
5
10
PKiKP/PcP = 0.0392, Epicentral Distance (deg) = 32.5514
PcP
Counts
2000
0
-2000
-10
-5
0
5
10
AK135 arrival time residual (s)

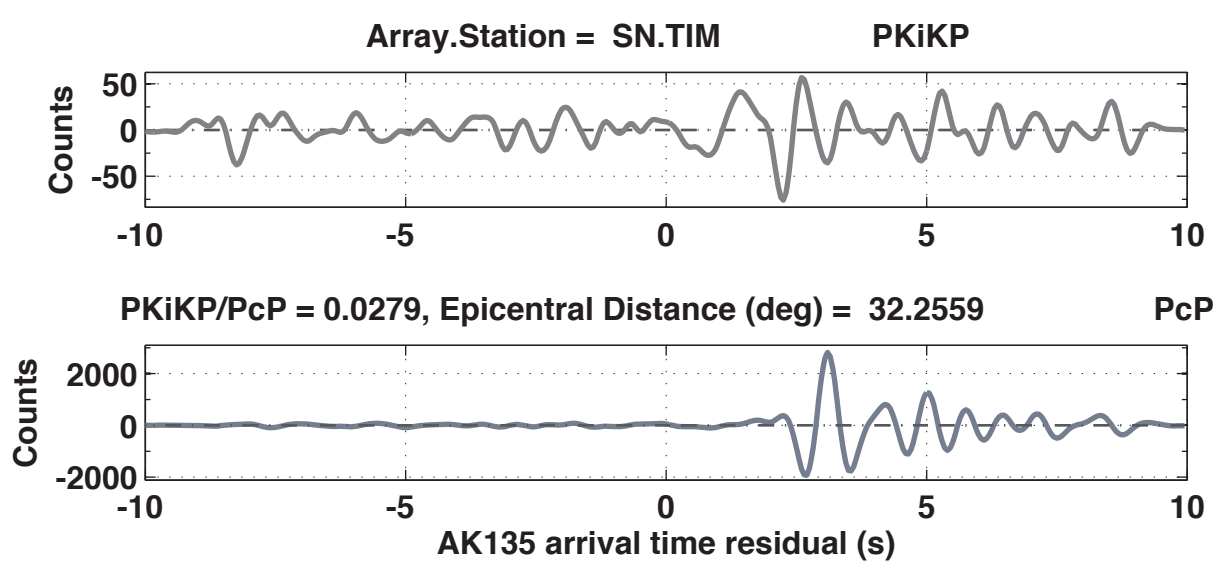
Array.Station = SN.TIM
PKiKP
Counts
50
0
-50
-10
-5
0
5
10
PKiKP/PcP = 0.0279, Epicentral Distance (deg) = 32.2559
PcP
Counts
2000
0
-2000
-10
-5
0
5
10
AK135 arrival time residual (s)

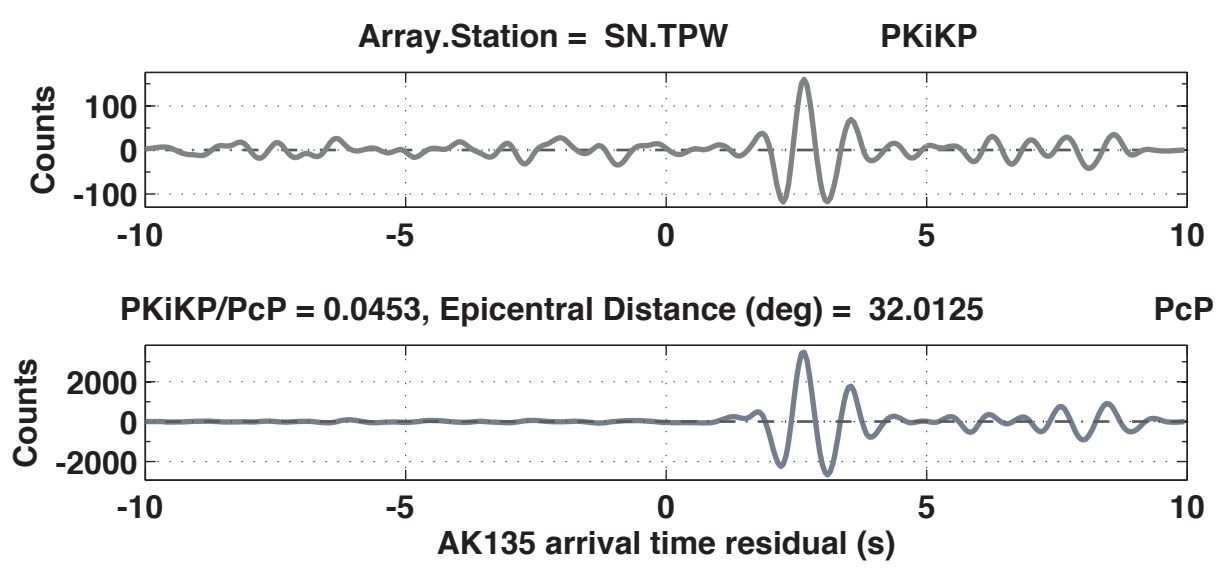
Array.Station = SN.TPW
PKiKP
Counts
100
0
-100
-10
-5
0
5
10
PKiKP/PcP = 0.0453, Epicentral Distance (deg) = 32.0125
PcP
Counts
2000
0
-2000
-10
-5
0
5
10
AK135 arrival time residual (s)

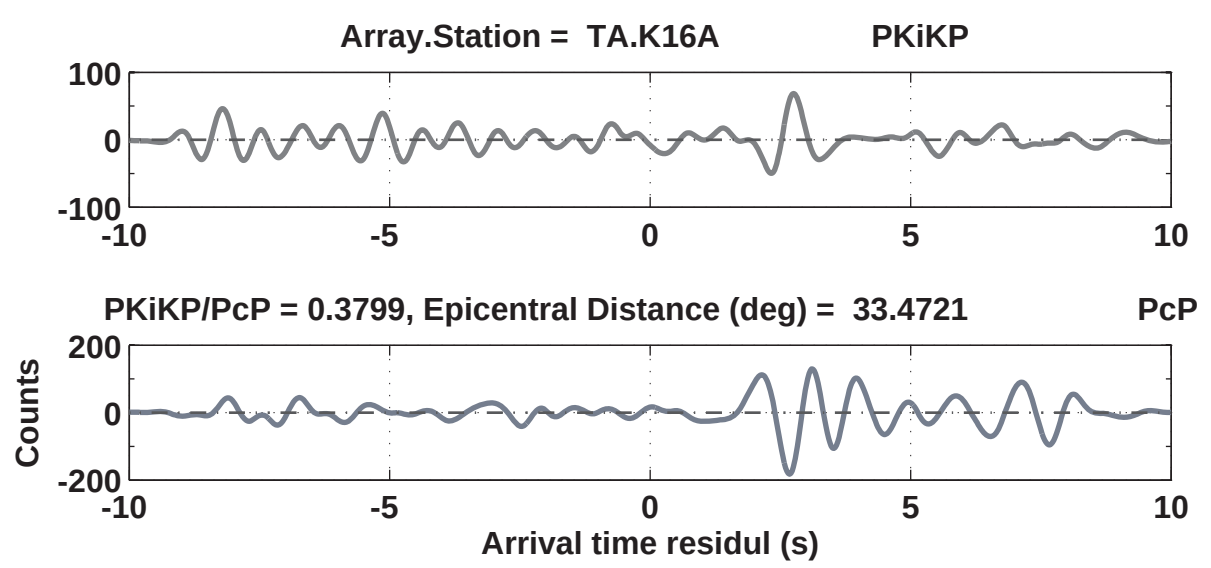
Array.Station = TA.K16A
PKiKP
100
0
-100
-10
-5
0
5
10
PKiKP/PcP = 0.3799, Epicentral Distance (deg) = 33.4721
PcP
200
0
-200
Counts
-10
-5
0
5
10
Arrival time residul (s)

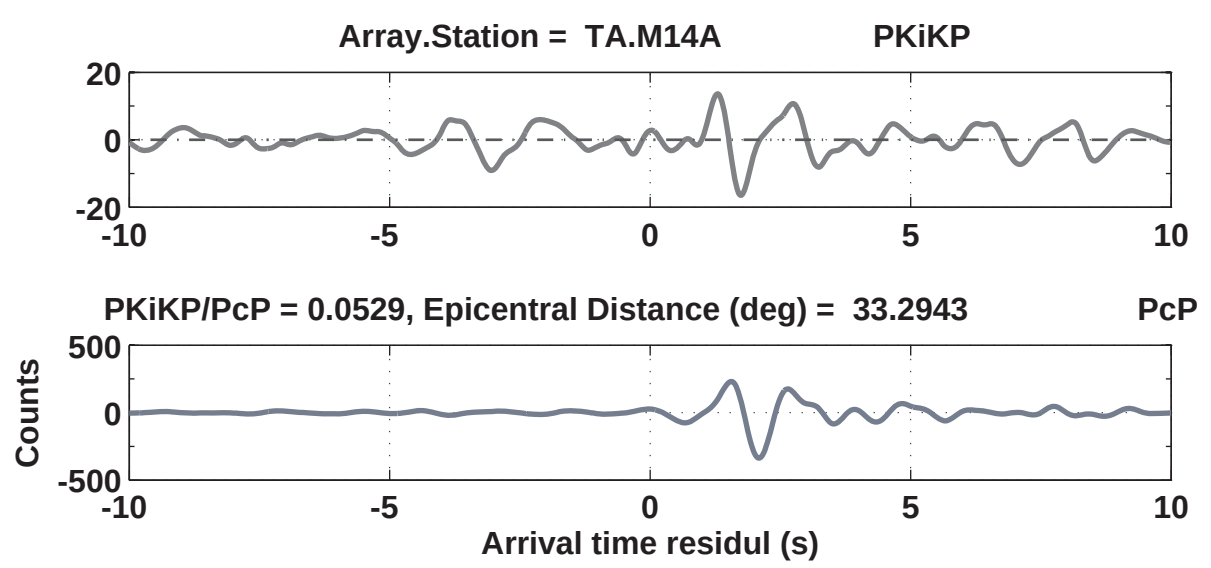
Array.Station = TA.M14A
PKiKP
20
0
-20
-10
-5
0
5
10
PKiKP/PcP = 0.0529, Epicentral Distance (deg) = 33.2943
PcP
500
0
-500
Counts
-10
-5
0
5
10
Arrival time residul (s)

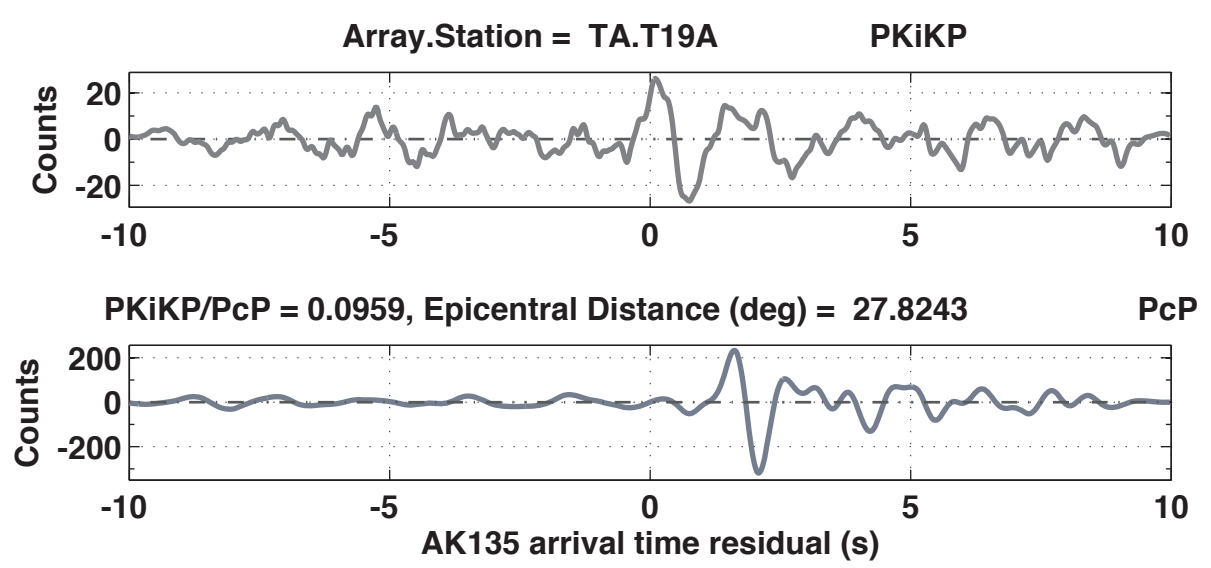
Array.Station = TA.T19A
PKiKP
Counts
20
0
-20
-10
-5
0
5
10
PKiKP/PcP = 0.0959, Epicentral Distance (deg) = 27.8243
PcP
Counts
200
0
-200
-10
-5
0
5
10
AK135 arrival time residual (s)

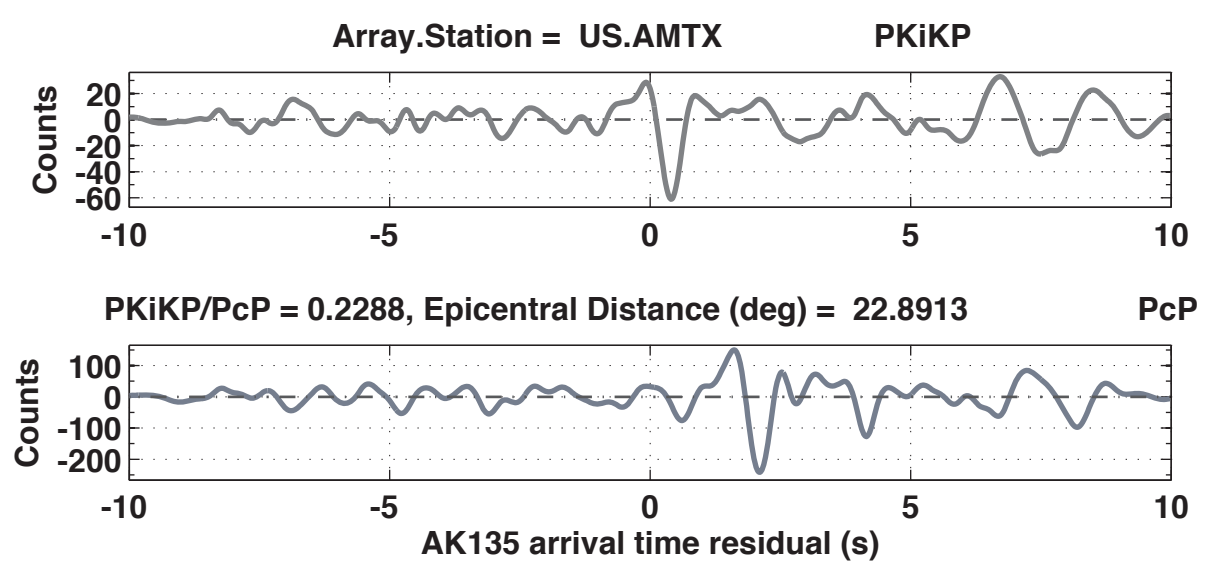
Array.Station = US.AMTX
PKiKP
Counts
20
0
-20
-40
-60
-10
-5
0
5
10
PKiKP/PcP = 0.2288, Epicentral Distance (deg) = 22.8913
PcP
Counts
100
0
-100
-200
-10
-5
0
5
10
AK135 arrival time residual (s)

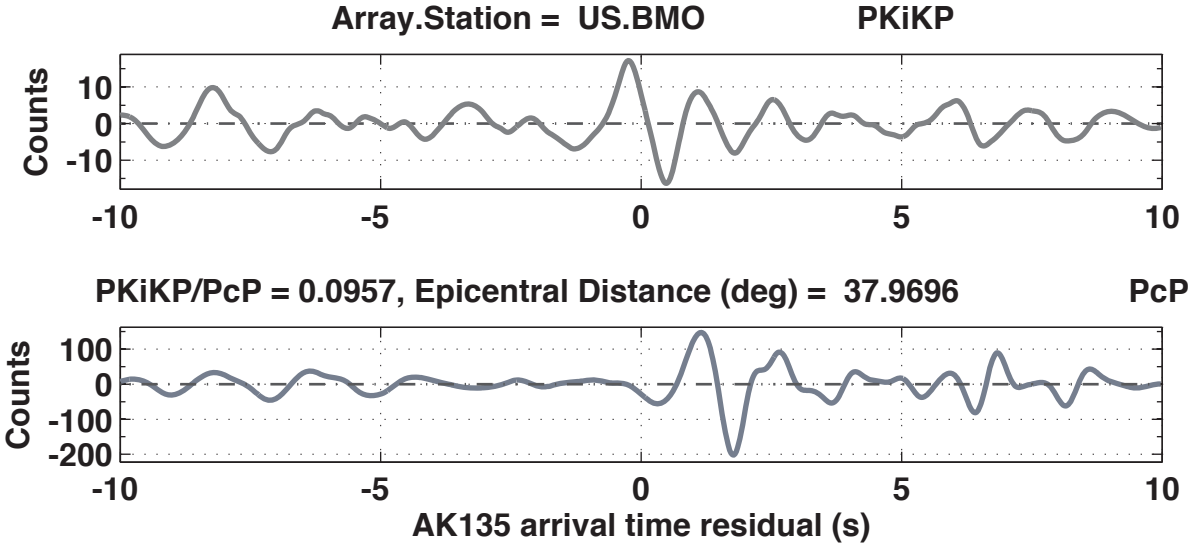
Array.Station = US.BMO
PKiKP
Counts
10
0
-10
-10
-5
0
5
10
PKiKP/PcP = 0.0957, Epicentral Distance (deg) = 37.9696
PcP
Counts
100
0
-100
-200
-10
-5
0
5
10
AK135 arrival time residual (s)

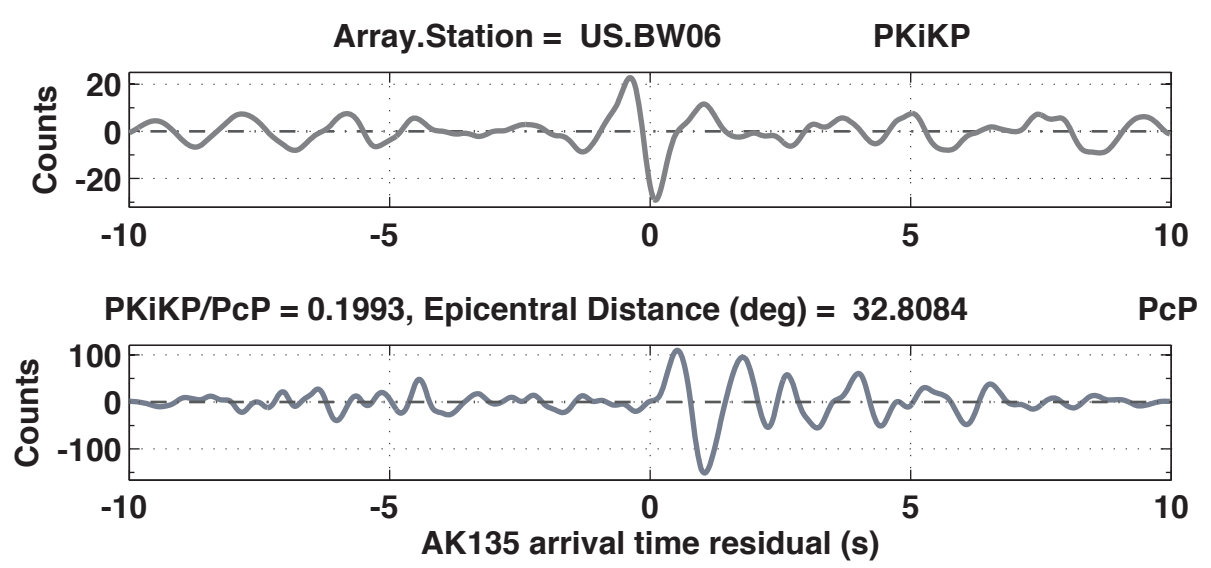
Array.Station = US.BW06
PKiKP
Counts
20
0
-20
-10
-5
0
5
10
PKiKP/PcP = 0.1993, Epicentral Distance (deg) = 32.8084
PcP
Counts
100
0
-100
-10
-5
0
5
10
AK135 arrival time residual (s)

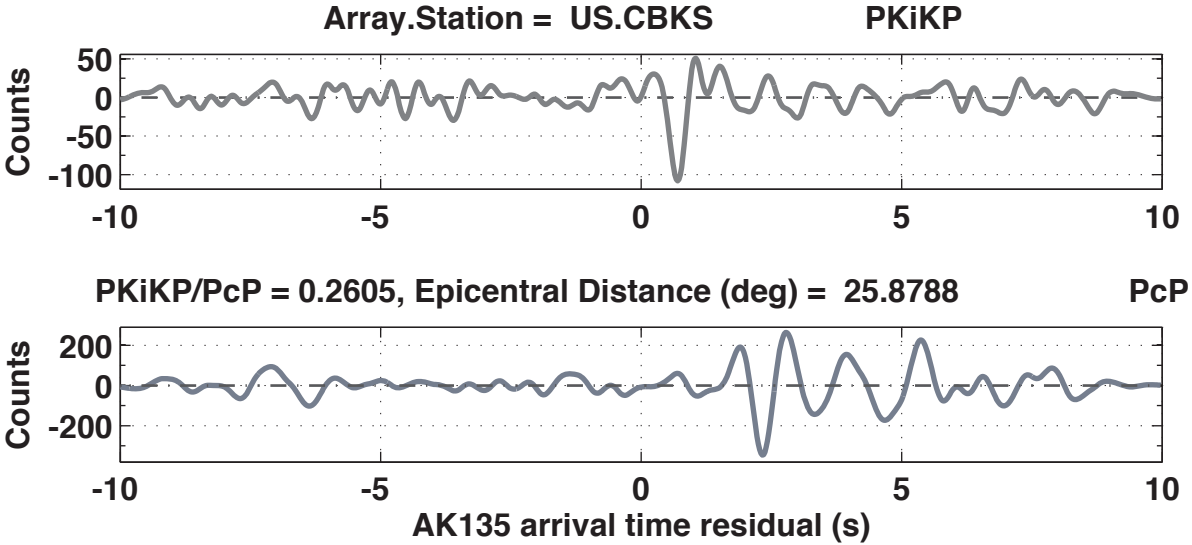
Array.Station = US.CBKS
PKiKP
Counts
50
0
-50
-100
-10
-5
0
5
10
PKiKP/PcP = 0.2605, Epicentral Distance (deg) = 25.8788
PcP
Counts
200
0
-200
-10
-5
0
5
10
AK135 arrival time residual (s)

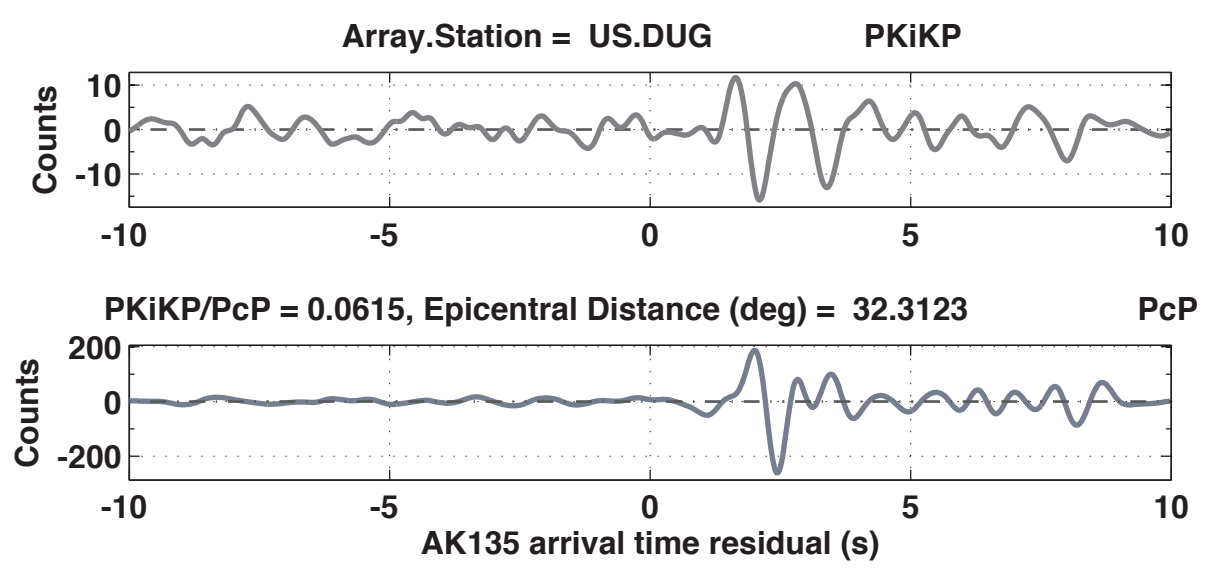
Array.Station = US.DUG
PKiKP
Counts
10
0
-10
-10
-5
0
5
10
PKiKP/PcP = 0.0615, Epicentral Distance (deg) = 32.3123
PcP
Counts
200
0
-200
-10
-5
0
5
10
AK135 arrival time residual (s)

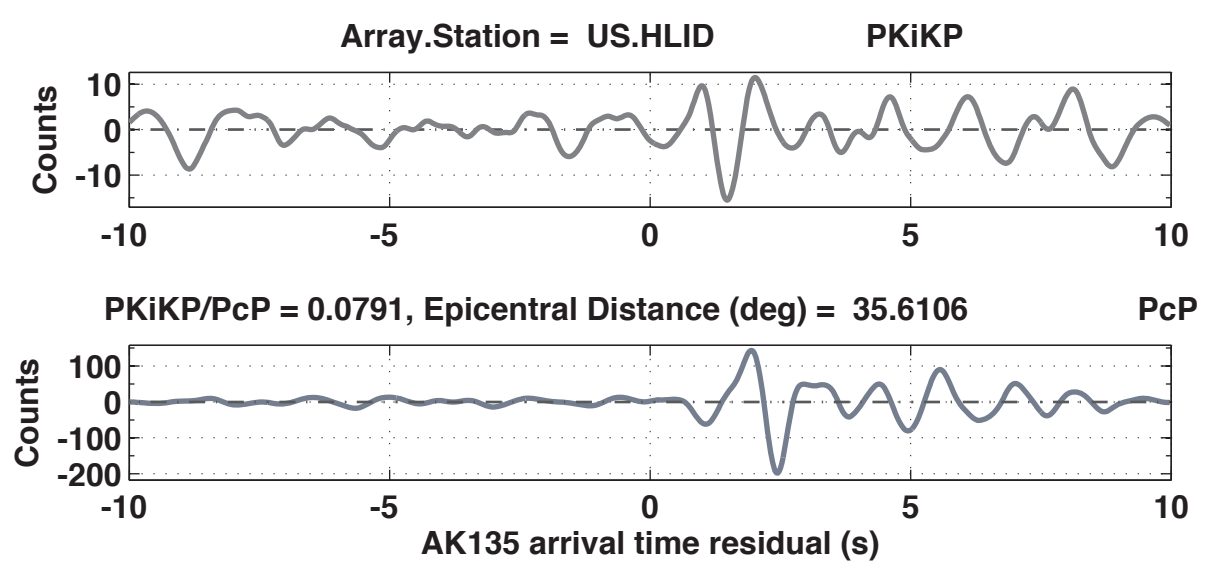
Array.Station = US.HLID
PKiKP
Counts
10
0
-10
-10
-5
0
5
10
PKiKP/PcP = 0.0791, Epicentral Distance (deg) = 35.6106
PcP
Counts
100
0
-100
-200
-10
-5
0
5
10
AK135 arrival time residual (s)

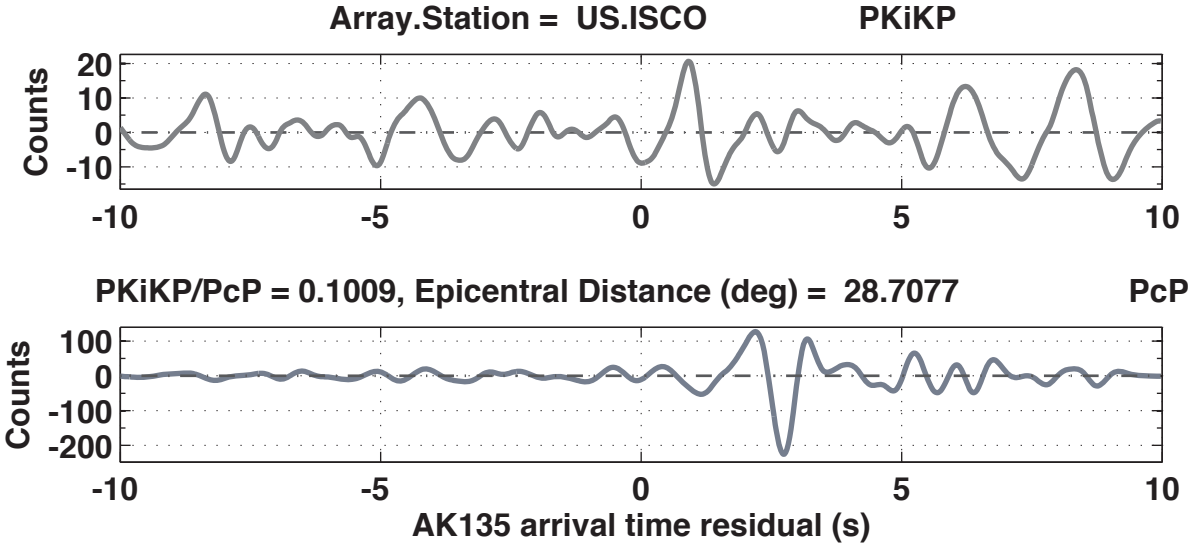
Array.Station = US.ISCO
PKiKP
Counts
20
10
0
-10
-10
-5
0
5
10
PKiKP/PcP = 0.1009, Epicentral Distance (deg) = 28.7077
PcP
Counts
100
0
-100
-200
-10
-5
0
5
10
AK135 arrival time residual (s)

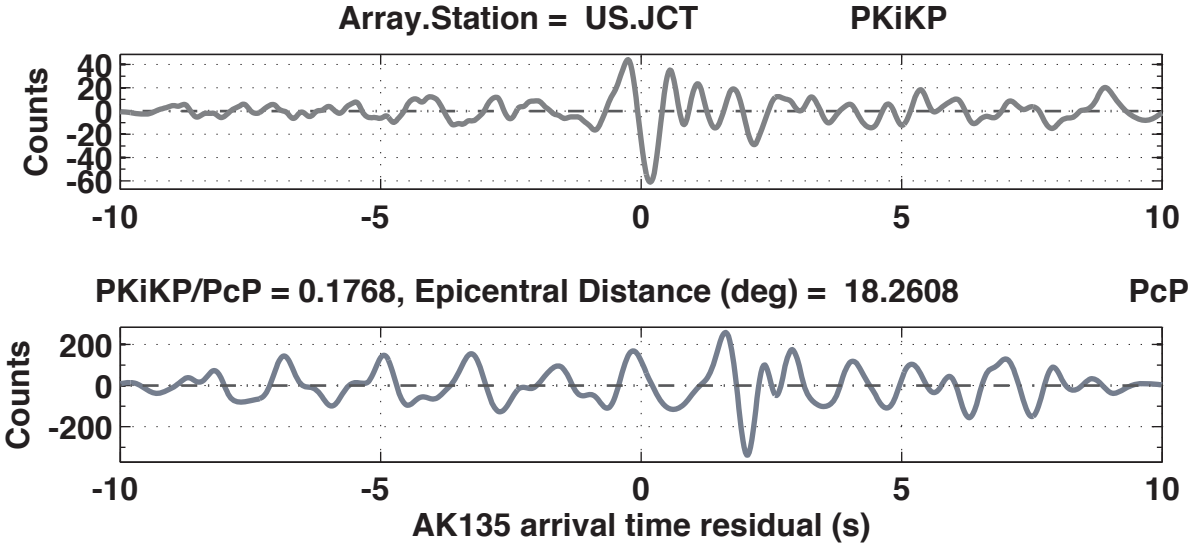
Array.Station = US.JCT
PKiKP
Counts
40
20
0
-20
-40
-60
-10
-5
0
5
10
PKiKP/PcP = 0.1768, Epicentral Distance (deg) = 18.2608
PcP
Counts
200
0
-200
-10
-5
0
5
10
AK135 arrival time residual (s)

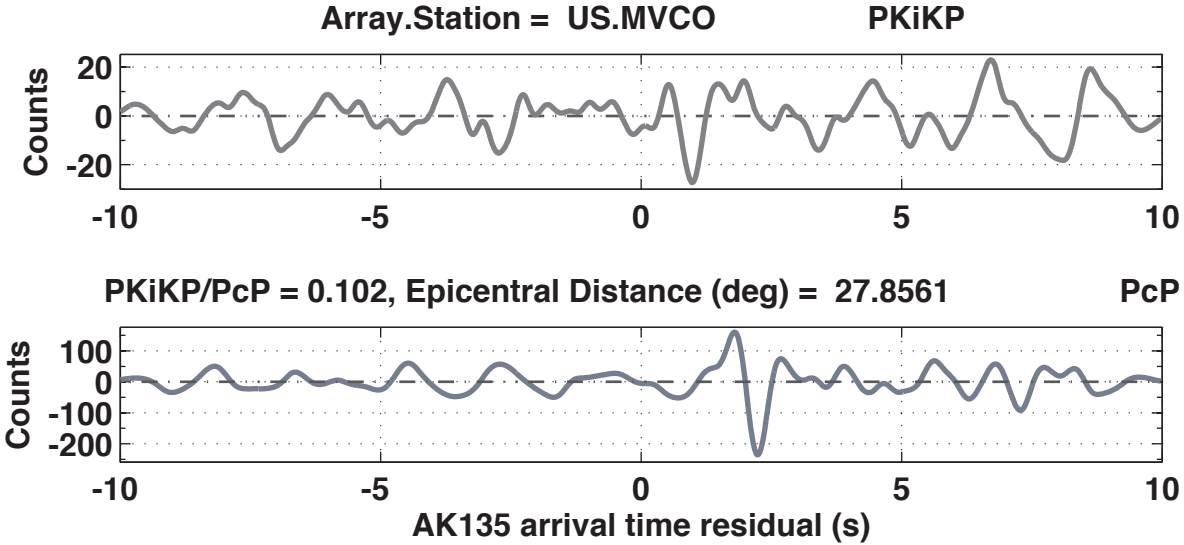
Array.Station = US.MVCO
PKiKP
Counts
20
0
-20
-10
-5
0
5
10
PKiKP/PcP = 0.102, Epicentral Distance (deg) = 27.8561
PcP
Counts
100
0
-100
-200
-10
-5
0
5
10
AK135 arrival time residual (s)

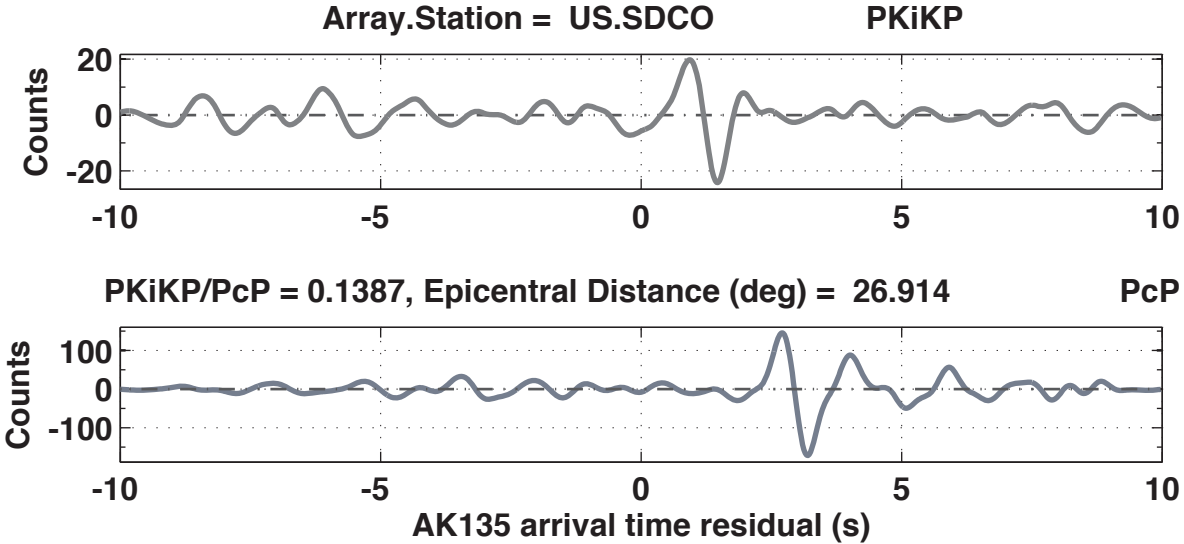
Array.Station = US.SDCO
PKiKP
Counts
20
0
-20
-10
-5
0
5
10
PKiKP/PcP = 0.1387, Epicentral Distance (deg) = 26.914
PcP
Counts
100
0
-100
-10
-5
0
5
10
AK135 arrival time residual (s)

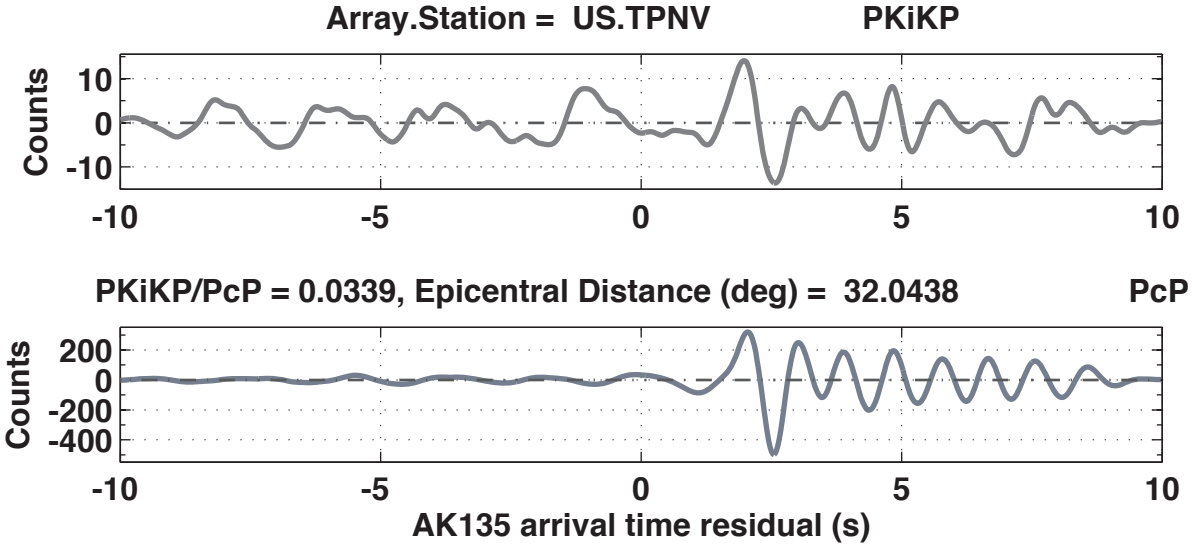
Array.Station = US.TPNV
PKiKP
Counts
10
0
-10
-10
-5
0
5
10
PKiKP/PcP = 0.0339, Epicentral Distance (deg) = 32.0438
PcP
Counts
200
0
-200
-400
-10
-5
0
5
10
AK135 arrival time residual (s)

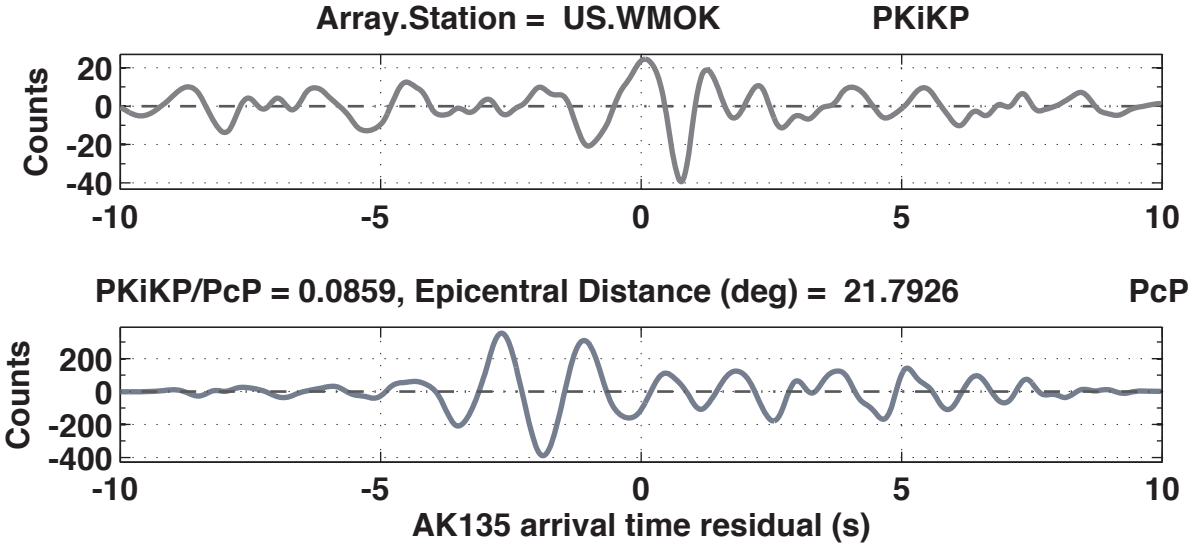
Array.Station = US.WMOK
PKiKP
Counts
20
0
-20
-40
-10
-5
0
5
10
PKiKP/PcP = 0.0859, Epicentral Distance (deg) = 21.7926
PcP
Counts
200
0
-200
-400
-10
-5
0
5
10
AK135 arrival time residual (s)

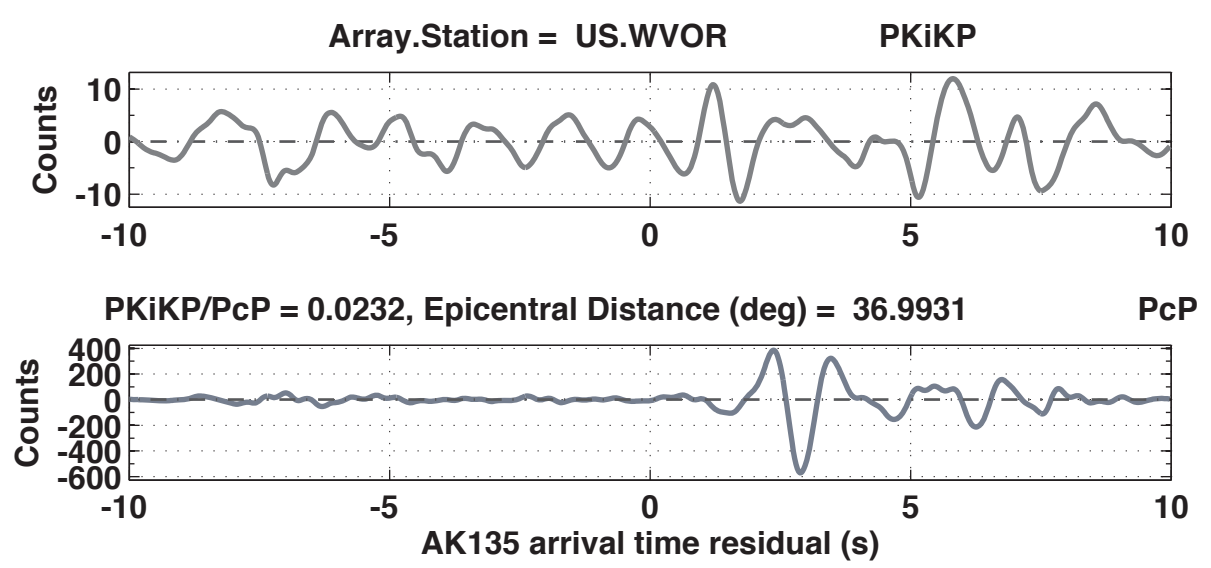
Array.Station = US.WVOR
PKiKP
Counts
10
0
-10
-10
-5
0
5
10
PKiKP/PcP = 0.0232, Epicentral Distance (deg) = 36.9931
PcP
Counts
400
200
0
-200
-400
-600
-10
-5
0
5
10
AK135 arrival time residual (s)

Array	Station	Latitude	Longitude
US	AMTX	34.88	-101.68
US	BMO	44.85	-117.31
US	BW06	42.77	-109.56
US	CBKS	38.81	-99.74
US	DUG	40.2	-112.81
US	SDCO	37.75	-105.5
US	TPNV	36.95	-116.25
US	WMOK	34.74	-98.78
US	WVOR	42.43	-118.64
US	HLID	43.56	-114.41
US	ISCO	39.8	-105.61
US	MVCO	37.21	-108.5
US	JCT	30.48	-99.8
SC	LEM	34.17	-106.97
SC	SBY	33.98	-107.18
SN	AMD	36.45	-116.28
SN	DOM	37	-116.41
SN	LEC	36.56	-116.69
SN	SGR	36.98	-117.03
SN	TIM	37.07	-116.47
SN	TPW	36.9	-116.25
TA	K16A	42.83	-111.59
TA	T19A	36.83	-109.02
TA	M14A	41.5	-113.35
CI	FUR	36.47	-116.86
CI	GMR	34.78	-115.66
CI	ISA	35.66	-118.47
CI	LRL	35.48	-117.68
CI	MPM	36.06	-117.49
CI	RDM	33.63	-116.85
CI	SHO	35.9	-116.28
CI	TUQ	35.44	-115.92